
OPERATOR LEARNING FOR SCHRÖDINGER EQUATION: UNITARITY, ERROR BOUNDS, AND TIME GENERALIZATION

Yash Patel*

Department of Statistics
University of Michigan
Ann Arbor, Michigan
yppatel.umich.edu

Unique Subedi*

Department of Statistics
University of Michigan
Ann Arbor, Michigan
subedi.umich.edu

Ambuj Tewari

Department of Statistics
University of Michigan
Ann Arbor, Michigan
tewaria.umich.edu

ABSTRACT

We consider the problem of learning the evolution operator for the time-dependent Schrödinger equation, where the Hamiltonian may vary with time. Existing neural network-based surrogates often ignore fundamental properties of the Schrödinger equation, such as linearity and unitarity, and lack theoretical guarantees on prediction error or time generalization. To address this, we introduce a linear estimator for the evolution operator that preserves a weak form of unitarity. We establish both upper and lower bounds on the prediction error that hold uniformly over all sufficiently smooth initial wave functions. Additionally, we derive time generalization bounds that quantify how the estimator extrapolates beyond the time points seen during training. Experiments across real-world Hamiltonians- including hydrogen atoms, ion traps for qubit design, and optical lattices- show that our estimator achieves relative errors 10^{-2} to 10^{-3} times smaller than state-of-the-art methods such as the Fourier Neural Operator and DeepONet.

1 Introduction

Solving the time-dependent Schrödinger equation is of interest in various engineering applications, including material science [1, 2] and the design of quantum computers [3, 4]. In all but the simplest cases, solving this equation requires numerical methods, which are computationally expensive even for a single initial condition [5, 6]. However, a single simulation is often insufficient for practical applications. For example, in qubit design, an essential requirement is that the system maintains coherence across a range of environmental conditions. This necessitates repeated simulations under varying initial conditions and system parameters, requiring significant computational resources [7, 8].

In fact, the need for repeated PDE solutions is widespread in engineering design, such as in simulating the Navier-Stokes equations for evaluating car or airfoil designs [9, 10]. To address this, operator learning has emerged as a promising approach for the surrogate modeling of PDEs, allowing efficient computation in such cases where repeated evaluation is required [11, 12]. Building on this idea, recent works have explored operator learning for accelerating solutions to the time-dependent Schrödinger equation [13, 14, 15]. These works, however, typically use general-purpose neural operators [16], most commonly the Fourier Neural Operator (FNO) [17], without explicitly using the special structure of the Schrödinger evolution, such as linearity and unitarity. In related fields, it has been demonstrated that incorporating known physical priors is often crucial for effective surrogate learning in data-scarce settings [18, 19].

Thus, in this work, we propose a surrogate model for the time-dependent Schrödinger equation that exploits the fundamental structures of this equation. Specifically, let F be the true evolution operator of the Schrödinger equation that maps the initial wave function ψ to its evolved state at some fixed time $T > 0$. We introduce an active data collection strategy and a *linear estimator* \hat{F} to approximate F and establish the following.

(i) **(Empirical Evaluation)** We evaluate \hat{F} across a range of Hamiltonians, including hydrogen atoms, double-slit potentials (see Figure 1), an ion trap used in qubit design, and optical lattices. Our estimator consistently outperforms neural operators baselines such as the FNO and DeepONet by 2 to 3 orders of magnitude, achieving relative errors

*Equal Contribution

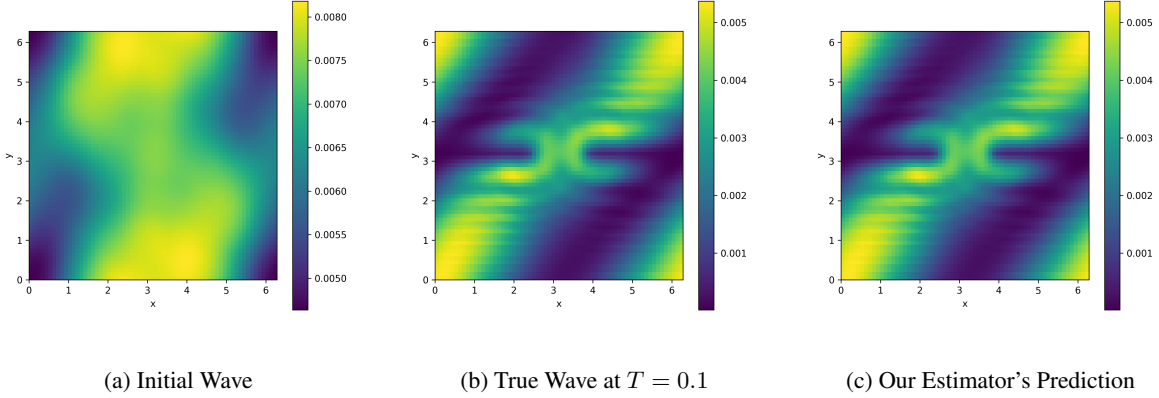


Figure 1: Squared amplitude $|\psi(x)|^2$ of the initial wave, the true wave at $T = 0.1$, and the estimator’s prediction for the barrier potential with double slits on $[0, 2\pi)^2$.

10^{-2} to 10^{-3} times smaller than these baselines.

(ii) **(Preservation of Physical Laws)** We prove that the surrogate \hat{F} preserves a weak form of unitarity, a fundamental property of the Schrödinger equation. Thus, our work aligns with broader efforts in physics-informed learning to incorporate known physical symmetries and conservation laws into model design and training [20, 21].

(iii) **(Theoretical Guarantees)** We prove upper and lower bounds on the prediction error of \hat{F} , establishing tight rates in terms of the number of training samples, the accuracy of the PDE solver used to generate training data, and the Sobolev smoothness of the initial wave function. Instead of bounding expected error with respect to some distribution that is common in statistical learning theory, we establish a stronger error guarantee that holds uniformly over smooth initial waves.

(iv) **(Time Generalization)** We establish time generalization bounds, showing that \hat{F} trained on data up to time point T can extrapolate to future time points $T' > T$ when the potential is time-independent and sufficiently smooth. While time generalization has been studied empirically in prior works on the Schrödinger equation [13, 15], little is known theoretically about when such generalization is possible. To the best of our knowledge, this work provides the first mathematical guarantees for time generalization in operator learning.

1.1 Related Works on Operator Learning and Time-Dependent Schrödinger Equation

One of the earlier works in this area was by [13], who used Fourier Neural Operators (FNOs) by [17] to estimate the evolution operator for simple quantum systems, including random potential functions and the double-slit potential. Additionally, they studied the time generalization ability of the learned operator by evolving the wave function beyond the time range included in the training dataset. Notably, their learned operator is more general as it maps from the initial wave function and potential function to the evolved state, rather than learning a propagator for a fixed Hamiltonian. A related work by [22] considers learning phases of amplitudes in scattering problems. While these works primarily study isolated quantum systems, [14] and [23] used FNO-based architectures to study dissipative quantum systems, where the system interacts with the surrounding environment and can be driven by external fields. They also assessed the time generalization capacity of the learned propagator. Recently, [15] used FNOs to learn the evolution operator of quantum spin systems and studied their ability for both single-step and multi-step time generalization. A more detailed discussion of related works is provided in Appendix A.

2 Preliminaries

Let \mathbb{R} and \mathbb{C} denote the real and complex numbers, respectively, while \mathbb{N} and \mathbb{Z} represent the natural numbers and integers. Define $\mathbb{N}_0 := \mathbb{N} \cup \{0\}$. For any $x \in \mathbb{R}^d$, the ℓ^p -norm is denoted by $|x|_p$. For $z \in \mathbb{C}$ with $z = a + bi$, define $|z| = \sqrt{a^2 + b^2}$. For $x, y \in \mathbb{R}^d$, the Euclidean inner product is denoted by $x \cdot y$. For two non-negative functions g and h defined on \mathbb{N} , we say $f \lesssim g$ if there exists a universal constant c and $n_0 \in \mathbb{N}$ such that $f(n) \leq cg(n)$ for all $n \geq n_0$. Equivalently, $f \gtrsim g$ means there exists a constant c and $n_0 \in \mathbb{N}$ such that $f(n) \geq cg(n)$ for all $n \geq n_0$.

Let $\Omega \subset \mathbb{R}^d$ be a bounded set. The space of square-integrable functions on Ω is defined as $L^2(\Omega) := \{u : \Omega \rightarrow \mathbb{C} \mid \int_{\Omega} |u(x)|^2 dx < \infty\}$. This is a Hilbert space with the inner product $\langle u, v \rangle_{L^2} = \int_{\Omega} u(x) \overline{v(x)} dx$, where $\bar{z} = a - bi$ is the complex conjugate of $z = a + bi$. The norm induced by this inner product is denoted by $\|\cdot\|_{L^2}$.

2.1 Time-Dependent Schrödinger Equation

The time-dependent Schrödinger equation states that the quantum system evolves as

$$i\hbar \partial_t \psi(\cdot, t) = H(t) \psi(\cdot, t).$$

Here, $\psi(\cdot, t) : \Omega \subseteq \mathbb{R}^d \rightarrow \mathbb{C}$ is the wave function at time point t , and $H(t)$ is the Hamiltonian operator that can evolve over time. For a single particle system, we generally have $d \in \{1, 2, 3\}$, and the Hamiltonian can be written as $H(t) = -\frac{\hbar^2}{2m} \Delta + V_t(\cdot)$, where $V_t(\cdot)$ is a time-dependent potential function and Δ is the Laplacian operator defined as $\Delta f := \sum_{j=1}^d \frac{\partial^2 f}{\partial x_j^2}$ for Euclidean coordinates.

The solution operator, also referred to as the time evolution operator, of the Schrödinger equation takes the form $\mathcal{T} \left[\exp \left(-\frac{i}{\hbar} \int_{t_0}^t H(s) ds \right) \right]$. That is, given an initial wave $\psi(\cdot, t_0)$ at time t_0 , the wave function at time point $t > t_0$ is given by $\psi(\cdot, t) = \mathcal{T} \left[\exp \left(-\frac{i}{\hbar} \int_{t_0}^t H(s) ds \right) \right] \psi(\cdot, t_0)$. Here, \mathcal{T} denotes the time-ordering operator, which ensures that Hamiltonians at different time points are applied in the correct temporal sequence. This ordering is necessary because the time-varying Hamiltonians do not generally commute at different times. One can formally define this operator in terms of a Dyson series expansion [24, Chapter 2]. When the Hamiltonian is constant over time, $H(t) = H$, the evolution operator has a more familiar form $\exp \left(-\frac{i(t-t_0)}{\hbar} H \right)$. While the solution operator has a closed-form representation, it is generally impractical for computation, as evaluating operator exponentials requires computing higher-order powers of the Hamiltonian and summing an infinite series in its Taylor expansion.

2.2 Problem Formulation and Goal

Define $t_0 = 0$ without loss of generality. For a fixed time $T > 0$, we seek to learn the operator

$$F := \mathcal{T} \left[\exp \left(-\frac{i}{\hbar} \int_0^T H(s) ds \right) \right].$$

Given a collection of n observed samples $\{(\psi_j(\cdot, 0), \psi_j(\cdot, T))\}_{j=1}^n$, where each sample satisfies $\psi_j(\cdot, T) = F(\psi_j(\cdot, 0))$, our goal is to construct an estimate \hat{F}_n that approximates F accurately under a suitable metric. More precisely, we want to develop a data generation strategy and an estimation rule such that the error of the estimator,

$$\sup_{\psi \in \mathcal{V}} \|\hat{F}_n(\psi) - F(\psi)\|_{L^2},$$

is small. Here, \mathcal{V} is some suitable subset of $L^2(\Omega)$ (consisting of, say, Sobolev-type smooth functions) that will be specified later. Note that our goal is to provide a *uniform error bound* over \mathcal{V} rather than a bound on expected error that is more common in statistical learning theory. This stronger guarantee is possible in our setting because we can evaluate $F(\psi)$ for any chosen initial wave function ψ , up to certain numerical accuracy, using a PDE solver. This flexibility allows us to actively select the most informative queries for constructing the estimator, rather than relying on the i.i.d. sampling typically used in statistical learning.

3 Data Collection Strategy and Estimator

In this section, we introduce our data generation strategy and define our estimation rule. Then, we establish the unitarity of the proposed estimator. For clarity of exposition, we assume that $\Omega = \mathbb{T}^d$, the d -dimensional torus [25, Chapter 3]. Extension to non-periodic domains is straightforward and is discussed in Section B. Throughout this paper, we identify \mathbb{T}^d by $[0, 1]^d$ equipped with periodic boundary conditions. Before moving forward, we first define the Sobolev space on \mathbb{T}^d . The theoretical guarantees established in this work apply only to initial waves that belong to these Sobolev spaces on \mathbb{T}^d or their equivalent counterparts in more general domains Ω .

For any $k \in \mathbb{Z}^d$, define the function $\varphi_k : \mathbb{T}^d \rightarrow \mathbb{C}$ by $\varphi_k(x) := e^{2\pi i k \cdot x}$. Using these functions, for any $s > 0$, we can define the Sobolev space as

$$\mathcal{H}^s(\mathbb{T}^d) := \left\{ f \in L^2(\mathbb{T}^d) : \sum_{k \in \mathbb{Z}^d} (1 + |k|_2^2)^s |\langle f, \varphi_k \rangle_{L^2}|^2 < \infty \right\}.$$

This space is equipped with the norm $\|f\|_{\mathcal{H}^s} := \sqrt{\sum_{k \in \mathbb{Z}^d} (1 + |k|_2^2)^s |\langle f, \varphi_k \rangle_{L^2}|^2}$. Although $\mathcal{H}^s(\mathbb{T}^d)$ is a Hilbert space, we will not rely on its Hilbertian properties in this work. When $s \in \mathbb{N}$, this definition of the Sobolev space is equivalent to its formulation based on derivatives. That is, $\mathcal{H}^s(\mathbb{T}^d) \simeq \left\{ f \in L^2(\mathbb{T}^d) \mid \sum_{|\alpha|_1 \leq s} \|D^\alpha f\|_{L^2}^2 < \infty \right\}$, where D^α denotes the differential operator. For more details on this equivalence, we refer the readers to [26, Chapter 4.3].

3.1 Estimator

Given a sample size budget of n such that $n \geq 3^d$, define $K_n := (n^{\frac{1}{d}} - 1)/2$. The estimator is constructed by querying a PDE solver to obtain $w_k = P(\varphi_k)$ for each $k \in \mathbb{Z}^d$ such that $|k|_\infty \leq K_n$, where P denotes the numerical PDE solver for the corresponding solution operator F of the Schrödinger equation. Since the number of such frequency indices satisfies $|\{k \in \mathbb{Z}^d : |k|_\infty \leq K_n\}| = (2\lfloor K_n \rfloor + 1)^d \leq n$, the sample budget of n is not exceeded. Using the labeled dataset $\{(\varphi_k, w_k)\}_{|k|_\infty \leq K_n}$, we then define the estimator

$$\hat{F}_n := \sum_{k \in \mathbb{Z}^d : |k|_\infty \leq K_n} w_k \otimes \varphi_k. \quad (1)$$

Here, $w \otimes v$ denotes a rank-one operator, defined for any $u \in L^2(\mathbb{T}^d)$ as $(w \otimes v)(u) = w \langle u, v \rangle_{L^2}$. Note that this estimator naturally extends to general domains Ω . For general Ω , one can query the eigenfunctions of the Laplacian operator. Recall that φ_k are the eigenfunctions for \mathbb{T}^d . For more complex domains, the estimator can also be constructed using alternative domain-specific algebraic bases, such as orthogonal polynomials or wavelets. See Appendix B for a more detailed discussion.

Remark. The estimator in Equation 1 is closely related to the approach of [27], who proposed a similar data collection strategy and estimator to highlight the advantages of active data collection in operator learning. However, their error guarantees hold only in expectation over input samples drawn from a distribution, whereas we establish a uniform bound. While our results are stated for the F , the error rates in Section 4 apply to any bounded linear operator, making our work a strict generalization of [27]. Furthermore, using the structure of the time-dependent Schrödinger equation, we establish additional properties such as weak unitarity and time generalization in this work, which do not necessarily hold for general linear operators.

3.2 On Unitarity of the Estimator

A key property of the Schrödinger equation is the unitarity of F . More precisely, F is a surjective operator on $L^2(\mathbb{T}^d)$ that preserves inner products, meaning $\langle F u, F v \rangle_{L^2} = \langle u, v \rangle_{L^2}$, $\forall u, v \in L^2(\mathbb{T}^d)$. A direct consequence of this is that the L^2 -norm remains invariant under evolution, $\|F(\psi)\|_{L^2}^2 = \|\psi\|_{L^2}^2$. This property is fundamental because, when interpreting $|\psi(x, t)|^2$ as the probability density of a particle's position, unitarity ensures that the total probability is conserved over time. Given this, it is natural to ask whether our estimator also satisfies unitarity.

Strictly speaking, \hat{F}_n is not fully unitary. For instance, if φ_ℓ is a Fourier mode with $\|\ell\|_\infty > K_n$, then $\hat{F}_n \varphi_\ell = 0$ despite $\|\varphi_\ell\|_{L^2} = 1$. However, \hat{F}_n satisfies a weaker form of unitarity, as captured in the following proposition (proof deferred to Appendix C).

Proposition 3.1. *Suppose the solver satisfies $\langle P(v), P(u) \rangle_{L^2} = \langle u, v \rangle_{L^2}$. Then, the following hold.*

- (i) *For all $u, v \in \text{span}(\{\varphi_k : |k|_\infty \leq K_n\})$, we have $\langle \hat{F}_n(u), \hat{F}_n(v) \rangle_{L^2} = \langle u, v \rangle_{L^2}$.*
- (ii) *For any $u \in L^2(\mathbb{T}^d)$, we have $\|\hat{F}_n(u)\|_{L^2} \leq \|u\|_{L^2}$.*

The first property shows that \hat{F}_n preserves inner products within the span of the Fourier modes used in its construction. However, the estimator may still not be fully unitary as the spans of φ_k and w_k for $|k|_\infty \leq K_n$ may differ, violating the surjectivity requirement. Nonetheless, property (i) ensures that the estimator preserves the L^2 norm within this

subspace. Although \hat{F}_n may not preserve the L^2 norm outside this span, the second property shows that it always acts as a contraction. This property is crucial for establishing the time generalization behavior of the estimator in Section 5. Finally, we note that the assumption $\langle P(v), P(v) \rangle_{L^2} = \langle u, v \rangle_{L^2}$ holds for many standard numerical solvers for the Schrödinger equation, such as the Crank-Nicolson and operator splitting methods.

4 Error Analysis and Convergence Rates

A meaningful guarantee for the estimator \hat{F}_n requires a guarantee on the accuracy of the PDE solver P used to approximate F . To that end, we impose the following assumption on the solver's accuracy.

Assumption 4.1. The learner has black-box access to F through an ε -accurate PDE solver P , which satisfies $\sup_{P_k \in \mathbb{Z}^d} \|P(\varphi_k) - F(\varphi_k)\|_{L^2} \leq \varepsilon$.

4.1 Upper Bounds

Under this assumption, we establish the following upper bound on the error of the estimator.

Theorem 4.2 (Upper Bound). *Under Assumption 4.1, the estimator defined in Equation (1) satisfies*

$$\|\hat{F}_n(\psi) - F(\psi)\|_{L^2} \leq \|\psi\|_{\mathcal{H}^s} (\varepsilon \gamma_n + 3^s n^{-\frac{s}{d}})$$

for every wave function $\psi \in \mathcal{H}^s(\mathbb{T}^d)$. Here, $\gamma_n \lesssim 1$ when $2s > d$, $\gamma_n \lesssim \sqrt{\log n}$ when $2s = d$, and $\gamma_n \lesssim n^{\frac{1}{2} - \frac{s}{d}}$ when $2s < d$.

The term $\varepsilon \gamma_n$ is the irreducible error, which remains nonzero as long as $\varepsilon > 0$. The second term $3^s n^{-s/d}$ is the estimation error, which vanishes as the sample size $n \rightarrow \infty$. This result shows that the estimation error vanishes at the rate $n^{-s/d}$ for every s and d . In the special case where $s > d/2$, the estimation error of $n^{-s/d}$ is always faster than the Monte Carlo rate of $n^{-1/2}$. This improvement is due to our data collection strategy, as described in Section 3.1, rather than standard i.i.d. sampling, which can never yield better than $n^{-1/2}$ convergence rate (at least for metric losses rather than its square). Finally, when the PDE solver is exact ($\varepsilon = 0$), we obtain the upper bound $\leq 3^s \|\psi\|_{\mathcal{H}^s} n^{-\frac{s}{d}}$ for every $s > 0$ regardless of d .

The proof of Theorem 4.2, provided in Appendix D, proceeds via a bias-variance type decomposition of the estimator's error. Each component of the decomposition is then bounded using the fact that $\psi \in \mathcal{H}^s(\mathbb{T}^d)$. It is worth noting that the assumption of Sobolev-type smoothness is implicitly present in many applied works on operator learning. See Appendix B.1 for a more detailed discussion.

4.2 Lower Bounds

A natural question that arises is whether these upper bounds are tight. This can be studied in two stages. First, can the bound be improved for the estimator defined in Section 3.1? Second, beyond this specific estimator, does the bound remain tight when considering all possible linear surrogates for the Schrödinger equation? Addressing the second question is more subtle, as establishing a meaningful information-theoretic lower bound requires precisely specifying the information accessible to the learner. The class of linear operators the learner is allowed to consider must be well-defined. One could argue that the PDE solver P itself serves as the surrogate, or in the most extreme case, that F is the optimal surrogate. Given these nuances, we leave the broader question of optimality to future work and focus here on studying the tightness of the bounds for our specific estimator \hat{F}_n . The lower bound on the error of our estimator is presented in Theorem 4.3 and its proof is deferred to Appendix E.

Theorem 4.3 (Lower Bound). *There exists a Hamiltonian H such that for any sample budget n and estimator \hat{F}_n defined in (1) obtained by querying an ε -approximate PDE solver for F , we can find a wave function ψ with $\|\psi\|_{\mathcal{H}^s} \leq 2$*

$$\text{such that } \|\hat{F}_n(\psi) - F(\psi)\|_{L^2} \gtrsim \begin{cases} \varepsilon + n^{-\frac{s}{d}}, & \text{if } 2s \geq d, \\ \varepsilon n^{\frac{1}{2}(\frac{1}{2} - \frac{s}{d})} + n^{-\frac{s}{d}} & \text{if } 2s < d. \end{cases}$$

This lower bound shows that the rate $n^{-s/d}$ is tight for reducible error. Additionally, even accounting for irreducible error, this bound matches the upper bound when $s > d/2$. For $s = d/2$, there remains a gap of $\sqrt{\log n}$, and the exponent is half in the regime $s < d/2$. Nonetheless, the result conclusively establishes that the irreducible error accumulates and grows to ∞ as n grows in the regime $s < d/2$. This introduces a tradeoff between sample size and reducible error, which is undesirable. Ideally, we want the error to decrease monotonically as n increases.

The proof of Theorem 4.3 is subtle and relies on the careful construction of both the Hamiltonian H and an ε -approximate solver for the true evolution operator F . The main challenge lies in constructing a test function ψ that simultaneously satisfies three key properties: (i) it is a valid wave function with unit L^2 -norm, (ii) it has bounded Sobolev norm, and (iii) it is sufficiently challenging that our estimator constructed from the training data incurs a large prediction error when applied to ψ .

4.3 Refined Upper Bound Under Stronger Assumptions on PDE Solver

The proof of the lower bound in Theorem 4.3 relies on constructing an adversarial PDE solver, raising the natural question of whether better error bounds are possible under more realistic solvers. So, we consider a setting where the PDE solver's errors behave like uncorrelated random noise, that is $\delta_k := F(\varphi_k) - P(\varphi_k)$ are uncorrelated random variables for different k 's. This setup parallels fixed-design regression under homoscedastic noise, although in our setting the learner actively chooses the design matrix. Under this assumption, we prove an improved upper bound (Theorem F.2), showing that the expected uniform error is $\leq \varepsilon + 3^s c n^{-\frac{s}{d}}$. We defer the technical details to Appendix F.

5 Time Generalization

In this section, we only consider the case where the Hamiltonian remains constant over time. Recall that the operator \hat{F}_n is trained to predict the wave function at time $t = T$. We now analyze the error when using it to evolve the initial wave function over multiple time steps, i.e., at $t = T, 2T, 3T, \dots$. For any $q \in \mathbb{N}$, the true wave function at time $t = qT$ is given by $\psi_{qT} = \exp(-i/\hbar \cdot qT H) \psi(\cdot, 0) = F^q(\psi(\cdot, 0))$. Here, we use the fact that $H(s) = H$ for all $s \geq 0$ and $F = \exp(-\frac{i}{\hbar} T H)$. Now, our goal is to quantify the deviation of the estimated evolution $\hat{F}_n^q(\psi)$ from the exact solution $F^q(\psi)$.

Theorem 5.1. *Suppose P satisfies $\langle P(u), P(v) \rangle_{L^2} = \langle u, v \rangle_{L^2}$. Let $\gamma_n \lesssim 1$ when $2s > d$, $\gamma_n \lesssim \sqrt{\log n}$ when $2s = d$, and $\gamma_n \lesssim n^{\frac{1}{2} - \frac{s}{d}}$ when $2s < d$. Then, for any $\psi \in \mathcal{H}^s(\mathbb{T}^d)$, the estimator (1) satisfies*

$$\|\hat{F}_n^q(\psi) - F^q(\psi)\|_{L^2} \leq (\varepsilon \gamma_n + 3^s n^{-\frac{s}{d}}) \sum_{j=0}^{q-1} \|F^j(\psi)\|_{\mathcal{H}^s}.$$

Theorem 5.1, whose proof is provided in Appendix G, establishes that the estimator \hat{F}_n can be used to evolve the wave function beyond the time range covered in the training set. However, this requires the true evolution operator to be sufficiently regular. Specifically, the estimator can evolve the wave function for $q - 1$ additional steps as long as $F^j(\psi) \in \mathcal{H}^s(\mathbb{T}^d)$ for all $j \leq q - 1$. This regularity requirement is natural, given that Theorem 4.2 already requires that the input belong to $\mathcal{H}^s(\mathbb{T}^d)$. However, instead of requiring $\hat{F}_n^j(\psi)$ to belong to $\mathcal{H}^s(\mathbb{T}^d)$, it is sufficient for $F^j(\psi)$ to be in $\mathcal{H}^s(\mathbb{T}^d)$. We also note that the linearity of the estimator \hat{F}_n plays a crucial role in the proof of Theorem 5.1. Equally important is the fact that \hat{F}_n is a contraction in L^2 (property (ii) of Proposition 3.1), which ensures that the time generalization bound does not suffer from worse convergence rates in terms of sample size or an exponential dependence on q . Thus, it is unclear whether similar guarantees could be derived for generic neural network-based surrogates. In fact, our empirical results suggest otherwise: our estimator exhibits significantly smaller time extrapolation error at step $j = 16$ than the single-step prediction error ($j = 1$) observed for neural operator surrogates (see Tables 2 and 3).

Although Theorem 5.1 provides a time generalization bound, it is expressed in terms of the rather abstract quantity $\|F^j(\psi)\|_{\mathcal{H}^s}$. Naturally, one may ask under what conditions this norm remains bounded. The following result bounds $\|F^j(\psi)\|_{\mathcal{H}^s}$ in terms of the properties of the potential function.

Corollary 5.2. *Suppose the ε -approximate PDE solver satisfies $\langle P(u), P(v) \rangle_{L^2} = \langle u, v \rangle_{L^2}$. Let $\gamma_n \lesssim 1$ when $2s > d$, $\gamma_n \lesssim \sqrt{\log n}$ when $2s = d$, and $\gamma_n \lesssim n^{\frac{1}{2} - \frac{s}{d}}$ when $2s < d$. Then, we have:*

(i) *If $V(x) = a \in \mathbb{R}$, then $\|\hat{F}_n^q(\psi) - F^q(\psi)\|_{L^2} \leq \|\psi\|_{\mathcal{H}^s} (\varepsilon \gamma_n + 3^s n^{-\frac{s}{d}}) q$.*

(ii) *If $V \in C^\infty(\mathbb{T}^d)$ is real-valued, then $\exists c > 0$ such that*

$$\|\hat{F}_n^q(\psi) - F^q(\psi)\|_{L^2} \leq \|\psi\|_{\mathcal{H}^s} (\varepsilon \gamma_n + 3^s n^{-\frac{s}{d}}) \cdot c q (1 + T(q - 1)).$$

(iii) *If $V \in \mathcal{H}^r(\mathbb{T}^d)$ for $r \geq \max\{s, d/2\}$, then $\exists c > 0$ such that*

$$\|\hat{F}_n^q(\psi) - F^q(\psi)\|_{L^2} \leq \|\psi\|_{\mathcal{H}^s} (\varepsilon \gamma_n + 3^s n^{-\frac{s}{d}}) \cdot \frac{\exp(c \|V\|_{\mathcal{H}^r} \cdot qT) - 1}{\exp(c \|V\|_{\mathcal{H}^r} \cdot T) - 1}.$$

Corollary 5.2 shows that time generalization is possible when the potential function V is sufficiently smooth. The extrapolation penalty varies with the regularity of V : it is linear in q when V is constant, grows polynomially when V is infinitely differentiable, and becomes exponential in q when V has only limited Sobolev regularity. Recall that $C^\infty(\mathbb{T}^d)$ are functions for which derivatives of all orders exist and are continuous. Notably, the convergence rate with respect to the sample size n remains unaffected. Our empirical findings suggest that the exponential dependence on q may be conservative, and improving this dependence on q remains an open question. Note that the dependence on V 's smoothness arises because, when V lacks regularity, the evolved wave function $F^j(\psi)$ may lose Sobolev smoothness. Since \hat{F}_n is recursively applied at each step, smoothness is needed to repeatedly invoke the one-step generalization guarantee. Without smoothness of V , time generalization would require a different estimator with small prediction error uniformly over all of $L^2(\mathbb{T}^d)$. However, such a stronger guarantee for one-step prediction likely requires a different structural assumption on V .

The proof of part (i) relies on the fact that φ_k 's are eigenfunctions of the Hamiltonian when V is constant. Part (ii) uses the seminal result due to [28]. The dependence on q can be sharpened to $q(1 + Tq)^\varepsilon$ for any $\varepsilon > 0$ using the refined estimate from [28]. For part (iii), we were unable to find a corresponding result in the literature for potentials V with limited Sobolev regularity (i.e., not C^∞). We therefore derive this estimate ourselves, adapting techniques from [28]. See Appendix H for the proof of Corollary 5.2.

6 Experiments

We now compare the generalization error of our proposed estimator to that of the Fourier Neural Operator and DeepONet surrogate models across several Hamiltonians of practical interest. Code is available at https://github.com/yashpate15400/schrodinger_op. We note that, while the time-evolution for a time-invariant Hamiltonian can theoretically be computed using a numerical solver for the time-independent Schrödinger equation to obtain eigenvalue-eigenfunction pairs $\{(E_k, \phi_k)\}_{|k|_\infty \leq K_n}$ (where we use ϕ in place of φ to explicitly note that ϕ need not be the Fourier modes) of Hamiltonian, fitting for any future queried initial condition $\psi(\cdot, 0)$ the coefficients $\{\alpha_k\}$ such that $\psi(\cdot, 0) = \sum_{|k|_\infty \leq K_n} \alpha_k \phi_k(\cdot)$, and finally estimating $\psi(\cdot, T) = \sum_{|k|_\infty \leq K_n} e^{-iE_k T/\hbar} \alpha_k \phi_k(\cdot)$, doing so is not feasible in all but the most trivial of Hamiltonians [29, 30]. In turn, learning a solution operator is of interest in both cases of time-invariant and time-dependent Hamiltonians, as we consider below.

In each of the experiments, we employed a standard second-order split-step pseudospectral method as the numerical solver P, where fields were solved in natural units, such that $\hbar = 1$ and $m = 1$ [31]. Experiments were conducted over \mathbb{T}^2 with a uniform discretization of 256×256 , with the exception of the Coulomb and dipole potentials, where solutions were sought over \mathcal{S}^2 , with $(\phi, \theta) \in [0, 2\pi) \times [0, \pi]$ discretized in an equiangular grid of size 64×32 . $K_n = 16$ was fixed across experiments, meaning the proposed estimator was fitted on $\mathcal{D} := \{(\varphi_k, P(\varphi_k))\}$ for $k \in \{-16, \dots, 0, \dots, 16\}^2$. For the Coulomb and dipole potentials, the estimator was fit on the spherical harmonics basis elements Y_ℓ^m for $\ell = 0, \dots, L_{\max}$ and $m = -\ell, \dots, \ell$, where $L_{\max} = 10$.

Initial conditions for test data were drawn from a Gaussian Random Field (GRF) by defining a field $\psi(\cdot, 0) = \sum_{|k|_\infty \leq N/2} c_k \varphi_k$, where $N/2$ is the Nyquist frequency and $c_k = Z\alpha^{1/2}(4\pi^2\|k\|_2^2 + \beta)^{-\gamma/2}$, where $Z \sim \mathcal{N}(0, 1)$, $\alpha = 1$, $\beta = 1$, and $\gamma = 4$. These are samples from a Gaussian distribution on $L^2(\mathbb{T}^d)$ with mean 0 and covariance operator $\alpha(-\Delta + \beta\mathbf{I})^{-\gamma}$. Similar draws were made for the Coulomb and dipole potentials, with the expansion being over $\{Y_\ell^m\}$ instead of $\{\varphi_k\}$.

As Fourier Neural Operators are intended to be trained on data drawn i.i.d. from the test distribution, we generated a separate training dataset $\mathcal{D}' := \{(\psi_i(\cdot, 0), P(\varphi_i))\}$ identically to the test points, such that $|\mathcal{D}'| = |\mathcal{D}|$. FNOs were fitted with K_n modes using Adam [32] for 20 epochs, where the complex fields were handled in the standard manner of representing the real and imaginary components as separate channels as in [13]. This setup was identically repeated for the DeepONet. We also tested FNO and DeepONet trained on basis function inputs rather than i.i.d. samples. However, its generalization was extremely poor as it uniformly predicted near-zero fields on test data. So, we restricted our comparisons to FNO and DeepONet models trained on i.i.d. samples.

For Coulomb and dipole potentials, we used the Spherical FNO proposed by [33]. Since no such extension to spherical domains exists, we exclude DeepONet from this comparison.

In each of the setups, a paired t-test was conducted on the relative error on the test points, defined as $\%_{\text{err}}^{(\text{est})} := \|\mathbf{P}(\psi(\cdot, 0)) - \hat{\mathbf{F}}_n(\psi(\cdot, 0))\|_{L^2} / \|\mathbf{P}(\psi(\cdot, 0))\|_{L^2}$, specifically testing the hypotheses

$$H_0 : \%_{\text{err}}^{(\text{lin})} = \%_{\text{err}}^{(\text{FNO})} \quad H_A : \%_{\text{err}}^{(\text{lin})} < \%_{\text{err}}^{(\text{FNO})} \quad (2)$$

Table 1: Summary of potentials implemented for experiments. Potentials without an explicit t dependency are time-independent. Full descriptions of these potentials as well as values chosen for the free parameters are provided in Appendix I.

Potential Name	Expression	Domain
Free Particle	$V(x, y) = 0$	\mathbb{T}^2
Barrier	$V(x, y) = \begin{cases} V_0 & \text{at } x = \pi, y \notin [\pi \pm w] \\ 0 & \text{else} \end{cases}$	\mathbb{T}^2
Harmonic Oscillator	$V(x, y) = \frac{1}{2}m\omega^2[(x - \pi)^2 + (y - \pi)^2]$	\mathbb{T}^2
Random Field	$V(x, y) \sim \text{GRF}(0, \alpha(-\Delta + \beta \mathbf{I})^{-\gamma})$	\mathbb{T}^2
Paul Trap	$V(x, y, t) = \left(\frac{U_0 + V_0 \cos(\omega t)}{r_0^2} \right) (x^2 + y^2)$	\mathbb{T}^2
Shaken Lattice	$V(x, y, t) = V_0 \cos[k(x - A \sin(\omega t))] + V_0 \cos(ky)$	\mathbb{T}^2
Gaussian Pulse	$V(x, y, t) = V_0 \exp\left(-\frac{(x-x_0)^2}{2\sigma_x^2} - \frac{(y-y_0)^2}{2\sigma_y^2}\right) \sum_{t_0} e^{-\frac{(t-t_0)^2}{2\sigma_t^2}}$	\mathbb{T}^2
Coulomb	$V(\theta, \phi) = -k \frac{e^2}{r^2}$	\mathcal{S}^2
Coulomb Dipole	$V(\theta, \phi) = V_0 \cos(\theta)$	\mathcal{S}^2

Table 2: Average relative errors across different Hamiltonians, computed over 100 i.i.d. test samples, with standard deviations in parentheses. p-values for the hypothesis test $H_A : \gamma_{\text{err}}^{(\text{lin})} < \gamma_{\text{err}}^{(\text{FNO})}$ are also provided. Note that, for the Coulomb and dipole potential, the FNO columns instead refer to SFNO models. Dashes for DeepONet indicate that it does not handle functions on a spherical domain.

	FNO	DeepONet	Linear	$\gamma_{\text{err}}^{(\text{lin})} < \gamma_{\text{err}}^{(\text{FNO})}$	$\gamma_{\text{err}}^{(\text{lin})} < \gamma_{\text{err}}^{(\text{DeepONet})}$
Free	6.313e-02 (6.497e-02)	1.643e-01 (1.440e-01)	1.113e-04 (1.189e-04)	6.71e-09	9.954e-11
Barrier	4.686e-02 (3.167e-02)	1.957e-01 (9.298e-02)	1.006e-04 (1.046e-04)	2.986e-14	6.082e-20
Harmonic Oscillator	3.898e-02 (1.544e-02)	1.359e-01 (5.018e-02)	8.861e-05 (4.532e-05)	3.306e-23	1.647e-24
Random	1.363e-02 (9.927e-03)	2.179e-01 (1.047e-01)	1.026e-04 (8.241e-05)	3.646e-13	9.784e-20
Paul Trap	1.029e-01 (4.559e-02)	5.214e-01 (6.61e-02)	8.8e-05 (5.973e-05)	3.57e-21	4.271e-46
Shaken Lattice	8.088e-02 (4.881e-03)	2.246e-01 (8.431e-02)	9.325e-05 (4.893e-05)	6.550e-62	3.4e-24
Gaussian Pulse	4.198e-02 (1.267e-02)	1.768e-01 (4.637e-02)	8.875e-05 (4.881e-05)	2.132e-28	3.786e-31
Coulomb	4.841e-02 (1.093e-02)	—	4.832e-05 (1.705e-05)	3.699e-34	—
Dipole	5.228e-02 (1.280e-02)	—	4.922e-05 (2.121e-05)	1.571e-32	—

A corresponding test was also performed for the DeepONet surrogate. We consider several Hamiltonians of interest from quantum mechanics, drawing examples from both classical settings and of recent research interest, summarized in Table 1 with full descriptions deferred to Appendix I.

The full set of results is presented in Table 2. From these results, we see that the proposed estimator significantly outperforms alternative operator learning methods across all the Hamiltonians, both time-independent and time-dependent, and over both the Fourier and spherical harmonics bases, by leveraging the known linear structure of the true solution operator. Notably, as discussed in the experimental setup, the test samples were drawn over the full spectrum, i.e., with modes defined up to the Nyquist frequency. So, the test samples can be outside the span of modes used to define the estimator. If, however, such test points are restricted to be in the span of the basis elements used to define the estimator, we observe the perfect recovery; such results are provided in Appendix J.

6.1 Time Generalization

To assess the time generalization of our estimator, we iteratively evolve the initial wave ψ as $\hat{\mathbb{F}}_n^j(\psi)$ for $j = 1, \dots, q$. Test initial conditions were sampled from a GRF, as described earlier. For each j and initial wave $\psi(\cdot, 0)$, we compute the relative error $\|P^j(\psi(\cdot, 0)) - \hat{\mathbb{F}}_n^j(\psi(\cdot, 0))\|_{L^2} / \|P^j(\psi(\cdot, 0))\|_{L^2}$. Table 3 presents the average relative errors, evaluated over a batch of 100 i.i.d. test samples.

For the free, harmonic oscillator, and random potential, the error remains nearly constant across time steps, indicating long-term generalization. A similar trend is observed for the Coulomb and dipole potentials on the sphere. In contrast, the error increases sharply, by three orders of magnitude at $j = 2$ for the barrier potential, which is likely due to its discontinuity. For time-dependent potentials such as the Paul trap, shaken lattice, and Gaussian pulse, the estimator incurs larger errors at later steps. Note that our time-generalization bounds do not apply to these time-varying Hamiltonians. Overall, the results show that our estimator generalizes well beyond the training time points for

Table 3: Average relative time-generalization errors across different Hamiltonians, computed over 100 i.i.d. test samples, with standard deviations shown in parentheses.

	$j = 1$	$j = 2$	$j = 4$	$j = 8$	$j = 16$
Free	1.029e-04 (1.045e-04)	1.029e-04 (1.045e-04)	1.029e-04 (1.045e-04)	1.029e-04 (1.045e-04)	1.029e-04 (1.045e-04)
Harmonic Oscillator	9.902e-05 (4.551e-05)	6.541e-04 (6.593e-05)	5.063e-04 (4.973e-05)	5.338e-04 (5.377e-05)	6.691e-04 (6.760e-05)
Random	1.025e-04 (9.682e-05)	1.025e-04 (9.683e-05)	1.025e-04 (9.684e-05)	1.025e-04 (9.688e-05)	1.025e-04 (9.706e-05)
Barrier	8.685e-05 (3.996e-05)	1.842e-02 (3.626e-03)	1.855e-02 (3.811e-03)	1.726e-02 (3.281e-03)	1.672e-02 (3.262e-03)
Paul Trap	9.396e-05 (4.715e-05)	1.467e-01 (1.766e-02)	4.424e-01 (4.988e-02)	6.230e-01 (5.038e-02)	6.563e-01 (4.718e-02)
Shaken Lattice	1.125e-04 (7.114e-05)	7.715e-02 (1.858e-03)	1.542e-01 (1.984e-02)	3.294e-01 (4.646e-02)	5.493e-01 (7.877e-02)
Gaussian Pulse	1.069e-04 (8.890e-05)	1.475e-02 (4.857e-03)	1.717e-02 (5.960e-03)	1.767e-02 (5.980e-03)	1.900e-02 (6.364e-03)
Coulomb	4.824e-05 (1.995e-05)	4.830e-05 (2.034e-05)	4.823e-05 (1.992e-05)	4.820e-05 (2.009e-05)	4.827e-05 (1.985e-05)
Dipole	4.727e-05 (1.463e-05)	4.789e-05 (1.455e-05)	4.829e-05 (1.455e-05)	4.733e-05 (1.380e-05)	5.116e-05 (1.528e-05)

sufficiently smooth potentials. Furthermore, the empirical error growth is notably slower than the exponential bound suggested in part (iii) of Corollary 5.2. We leave this possible refinement for future work.

7 Discussion

In this work, we introduced a linear operator surrogate to estimate the evolution operator of the time-dependent Schrödinger equation. While our method provides rigorous theoretical guarantees, it is currently limited to a single particle system. A natural direction for future work is to extend the method to handle a system with N -interacting particles. A wave function for N -particle system must be symmetric for Bosons or antisymmetric for Fermions. Thus, one approach could be to generalize our data generation and the estimator to enforce these constraints.

Additionally, our method estimates the evolution operator for a fixed Hamiltonian. An interesting extension would be to develop a surrogate that takes both the initial wave and the potential as inputs and predicts the wave function at time T . Such a method would allow generalization across different system configurations, which can be used in applications such as qubit design. However, this requires moving beyond linear operators, as the ground truth operator mapping from $(\psi(\cdot, 0), V)$ to $\psi(\cdot, T)$ is nonlinear. Constructing such nonlinear estimators with neural networks is relatively straightforward, but providing rigorous theoretical guarantees presents a significant challenge.

References

- [1] Wen-Hao Liu, Zhi Wang, Zhang-Hui Chen, Jun-Wei Luo, Shu-Shen Li, and Lin-Wang Wang. Algorithm advances and applications of time-dependent first-principles simulations for ultrafast dynamics. *Wiley Interdisciplinary Reviews: Computational Molecular Science*, 12(3):e1577, 2022.
- [2] Xiaosong Li, Niranjana Govind, Christine Isborn, A Eugene DePrince III, and Kenneth Lopata. Real-time time-dependent electronic structure theory. *Chemical Reviews*, 120(18):9951–9993, 2020.
- [3] Wael W Mohammed, Naveed Iqbal, S Bourazza, and Elsayed M Elsayed. The optical structures for the fractional chiral nonlinear schrödinger equation with time-dependent coefficients. *Optical and Quantum Electronics*, 56(9):1476, 2024.
- [4] Xiao Chen, Silas Hoffman, James N Fry, and Hai-Ping Cheng. Simulating decoherence of coupled two spin qubits using generalized cluster correlation expansion. *arXiv preprint arXiv:2402.18722*, 2024.
- [5] Uri Peskin and Nimrod Moiseyev. The solution of the time-dependent schrödinger equation by the (t, t') method: Theory, computational algorithm and applications. *The Journal of chemical physics*, 99(6):4590–4596, 1993.
- [6] W van Dijk, J Brown, and K Spyksma. Efficiency and accuracy of numerical solutions to the time-dependent schrödinger equation. *Physical Review E—Statistical, Nonlinear, and Soft Matter Physics*, 84(5):056703, 2011.
- [7] Chris Nagele, Oliver Janssen, and Matthew Kleban. Decoherence: a numerical study. *Journal of Physics A: Mathematical and Theoretical*, 56(8):085301, 2023.
- [8] Ning Wu, Arun Nanduri, and Herschel Rabitz. Rabi oscillations, decoherence, and disentanglement in a qubit–spin-bath system. *Physical Review A*, 89(6):062105, 2014.
- [9] Ava Shahrokhi and Alireza Jahangirian. Airfoil shape parameterization for optimum navier–stokes design with genetic algorithm. *Aerospace science and technology*, 11(6):443–450, 2007.
- [10] SİNAN Eyi, JO Hager, and KD Lee. Airfoil design optimization using the navier-stokes equations. *Journal of Optimization Theory and Applications*, 83:447–461, 1994.

- [11] Kamyar Azizzadenesheli, Nikola Kovachki, Zongyi Li, Miguel Liu-Schiaffini, Jean Kossaifi, and Anima Anandkumar. Neural operators for accelerating scientific simulations and design. *Nature Reviews Physics*, pages 1–9, 2024.
- [12] Yannick Augenstein, Taavi Repan, and Carsten Rockstuhl. Neural operator-based surrogate solver for free-form electromagnetic inverse design. *ACS Photonics*, 10(5):1547–1557, 2023.
- [13] Sebastian Mizera. Scattering with neural operators. *Physical Review D*, 108(10):L101701, 2023.
- [14] Jiaji Zhang, Carlos L Benavides-Riveros, and Lipeng Chen. Artificial-intelligence-based surrogate solution of dissipative quantum dynamics: physics-informed reconstruction of the universal propagator. *The Journal of Physical Chemistry Letters*, 15(13):3603–3610, 2024.
- [15] Freya Shah, Taylor L Patti, Julius Berner, Bahareh Tolooshams, Jean Kossaifi, and Anima Anandkumar. Fourier neural operators for learning dynamics in quantum spin systems. *arXiv preprint arXiv:2409.03302*, 2024.
- [16] Nikola Kovachki, Zongyi Li, Burigede Liu, Kamyar Azizzadenesheli, Kaushik Bhattacharya, Andrew Stuart, and Anima Anandkumar. Neural operator: Learning maps between function spaces with applications to pdes. *Journal of Machine Learning Research*, 24(89):1–97, 2023.
- [17] Zongyi Li, Nikola Kovachki, Kamyar Azizzadenesheli, Burigede Liu, Kaushik Bhattacharya, Andrew Stuart, and Anima Anandkumar. Fourier neural operator for parametric partial differential equations. *International Conference on Learning Representations*, 2021.
- [18] Simon Batzner, Albert Musaelian, Lixin Sun, Mario Geiger, Jonathan P Mailoa, Mordechai Kornbluth, Nicola Molinari, Tess E Smidt, and Boris Kozinsky. E (3)-equivariant graph neural networks for data-efficient and accurate interatomic potentials. *Nature communications*, 13(1):2453, 2022.
- [19] Amil Merchant, Simon Batzner, Samuel S Schoenholz, Muratahan Aykol, Gwooon Cheon, and Ekin Dogus Cubuk. Scaling deep learning for materials discovery. *Nature*, 624(7990):80–85, 2023.
- [20] Zongyi Li, Hongkai Zheng, Nikola Kovachki, David Jin, Haoxuan Chen, Burigede Liu, Kamyar Azizzadenesheli, and Anima Anandkumar. Physics-informed neural operator for learning partial differential equations. *ACM/JMS Journal of Data Science*, 1(3):1–27, 2024.
- [21] Jack Richter-Powell, Yaron Lipman, and Ricky TQ Chen. Neural conservation laws: A divergence-free perspective. *Advances in Neural Information Processing Systems*, 35:38075–38088, 2022.
- [22] Vasilis Niarchos and Constantinos Papageorgakis. Learning s-matrix phases with neural operators. *Physical Review D*, 110(4):045020, 2024.
- [23] Jiaji Zhang, Carlos L Benavides-Riveros, and Lipeng Chen. Neural quantum propagators for driven-dissipative quantum dynamics. *Physical Review Research*, 7(1):L012013, 2025.
- [24] Jun John Sakurai and Jim Napolitano. *Modern quantum mechanics*. Cambridge University Press, 2020.
- [25] Loukas Grafakos et al. *Classical fourier analysis*, volume 2. Springer, 2008.
- [26] Michael E Taylor. *Partial differential equations I basic theory*. 2011.
- [27] Unique Subedi and Ambuj Tewari. On the benefits of active data collection in operator learning. *arXiv preprint arXiv:2410.19725*, 2024.
- [28] Jean Bourgain. On growth of sobolev norms in linear schrödinger equations with smooth time dependent potential. *Journal d’Analyse Mathématique*, 77(1):315–348, 1999.
- [29] W Van Dijk and FM Toyama. Accurate numerical solutions of the time-dependent schrödinger equation. *Physical Review E—Statistical, Nonlinear, and Soft Matter Physics*, 75(3):036707, 2007.
- [30] Claude Leforestier, RH Bisseling, Charly Cerjan, MD Feit, Rich Friesner, A Guldborg, A Hammerich, G Jolicard, W Karrlein, H-D Meyer, et al. A comparison of different propagation schemes for the time dependent schrödinger equation. *Journal of Computational Physics*, 94(1):59–80, 1991.
- [31] J André C Weideman and Ben M Herbst. Split-step methods for the solution of the nonlinear schrödinger equation. *SIAM Journal on Numerical Analysis*, 23(3):485–507, 1986.
- [32] Diederik P Kingma and Jimmy Ba. Adam: A method for stochastic optimization. *arXiv preprint arXiv:1412.6980*, 2014.
- [33] Boris Bonev, Thorsten Kurth, Christian Hundt, Jaideep Pathak, Maximilian Baust, Karthik Kashinath, and Anima Anandkumar. Spherical fourier neural operators: Learning stable dynamics on the sphere. In *International conference on machine learning*, pages 2806–2823. PMLR, 2023.

- [34] Jan Hermann, James Spencer, Kenny Choo, Antonio Mezzacapo, W Matthew C Foulkes, David Pfau, Giuseppe Carleo, and Frank Noé. Ab initio quantum chemistry with neural-network wavefunctions. *Nature Reviews Chemistry*, 7(10):692–709, 2023.
- [35] Jannes Nys, Gabriel Pescia, Alessandro Sinibaldi, and Giuseppe Carleo. Ab-initio variational wave functions for the time-dependent many-electron schrödinger equation. *Nature communications*, 15(1):9404, 2024.
- [36] Karan Shah, Patrick Stiller, Nico Hoffmann, and Attila Cangi. Physics-informed neural networks as solvers for the time-dependent schrodinger equation. *arXiv preprint arXiv:2210.12522*, 2022.
- [37] Salvatore Cuomo, Vincenzo Schiano Di Cola, Fabio Giampaolo, Gianluigi Rozza, Maziar Raissi, and Francesco Piccialli. Scientific machine learning through physics–informed neural networks: Where we are and what’s next. *Journal of Scientific Computing*, 92(3):88, 2022.
- [38] Kyle Mills, Michael Spanner, and Isaac Tamblyn. Deep learning and the schrödinger equation. *Physical Review A*, 96(4):042113, 2017.
- [39] George Stepaniants. Learning partial differential equations in reproducing kernel hilbert spaces. *Journal of Machine Learning Research*, 24(86):1–72, 2023.
- [40] Nicolas Boullé, Christopher J Earls, and Alex Townsend. Data-driven discovery of green’s functions with human-understandable deep learning. *Scientific reports*, 12(1):4824, 2022.
- [41] Alessandro Bisio, Giulio Chiribella, Giacomo Mauro D’Ariano, Stefano Facchini, and Paolo Perinotti. Optimal quantum learning of a unitary transformation. *Physical Review A—Atomic, Molecular, and Optical Physics*, 81(3):032324, 2010.
- [42] Stephanie Hyland and Gunnar Rätsch. Learning unitary operators with help from u (n). In *Proceedings of the AAAI Conference on Artificial Intelligence*, volume 31, 2017.
- [43] Mikhail Gennadievich Belov and Vladislav Gennadievich Malyshev. Partially unitary learning. *Physical Review E*, 110(5):055306, 2024.
- [44] J Robert Johansson, Paul D Nation, and Franco Nori. Qutip: An open-source python framework for the dynamics of open quantum systems. *Computer physics communications*, 183(8):1760–1772, 2012.
- [45] Yi-Ming Huang, Xiao-Yu Li, Yi-Xuan Zhu, Hang Lei, Qing-Sheng Zhu, and Shan Yang. Learning unitary transformation by quantum machine learning model. *Computers, Materials & Continua*, 68(1), 2021.
- [46] Maarten V de Hoop, Nikola B Kovachki, Nicholas H Nelsen, and Andrew M Stuart. Convergence rates for learning linear operators from noisy data. *SIAM/ASA Journal on Uncertainty Quantification*, 11(2):480–513, 2023.
- [47] Mattes Mollenhauer, Nicole Mücke, and TJ Sullivan. Learning linear operators: Infinite-dimensional regression as a well-behaved non-compact inverse problem. *arXiv preprint arXiv:2211.08875*, 2022.
- [48] Gabriel J Lord, Catherine E Powell, and Tony Shardlow. *An introduction to computational stochastic PDEs*, volume 50. Cambridge University Press, 2014.
- [49] Kaushik Bhattacharya, Bamdad Hosseini, Nikola B Kovachki, and Andrew M Stuart. Model reduction and neural networks for parametric pdes. *The SMAI journal of computational mathematics*, 7:121–157, 2021.
- [50] Tailen Hsing and Randall Eubank. *Theoretical foundations of functional data analysis, with an introduction to linear operators*, volume 997. John Wiley & Sons, 2015.
- [51] Lu Lu, Pengzhan Jin, Guofei Pang, Zhongqiang Zhang, and George Em Karniadakis. Learning nonlinear operators via deeponet based on the universal approximation theorem of operators. *Nature machine intelligence*, 3(3):218–229, 2021.
- [52] Jean-Marc Delort. Growth of sobolev norms of solutions of linear schrödinger equations on some compact manifolds. *International Mathematics Research Notices*, 2010(12):2305–2328, 2010.
- [53] Ali Behzadan and Michael Holst. Multiplication in sobolev spaces, revisited. *Arkiv för Matematik*, 59(2):275–306, 2021.
- [54] Fouad G. Major, Viorica N. Gheorghe, and Günther Werth. *Charged Particle Traps: Physics and Techniques of Charged Particle Field Confinement*. Springer, 2005.
- [55] Francesco Bernardini, Abhijit Chakraborty, and Carlos R Ordóñez. Quantum computing with trapped ions: a beginner’s guide. *European Journal of Physics*, 45(1):013001, 2023.
- [56] Ivan H Deutsch, Gavin K Brennen, and Poul S Jessen. Quantum computing with neutral atoms in an optical lattice. *Fortschritte der Physik: Progress of Physics*, 48(9-11):925–943, 2000.

- [57] Chuanwei Zhang, SL Rolston, and S Das Sarma. Manipulation of single neutral atoms in optical lattices. *Physical Review A—Atomic, Molecular, and Optical Physics*, 74(4):042316, 2006.
- [58] Wei Zheng and Hui Zhai. Floquet topological states in shaking optical lattices. *Physical Review A*, 89(6):061603, 2014.
- [59] Anthony Kiely, Albert Benseny, Thomas Busch, and Andreas Ruschhaupt. Shaken not stirred: creating exotic angular momentum states by shaking an optical lattice. *Journal of Physics B: Atomic, Molecular and Optical Physics*, 49(21):215003, 2016.
- [60] CA Weidner, Hoon Yu, Ronnie Kosloff, and Dana Z Anderson. Atom interferometry using a shaken optical lattice. *Physical Review A*, 95(4):043624, 2017.
- [61] Jan Rais, Hendrik van Hees, and Carsten Greiner. Bound-state formation in time-dependent potentials. *Physical Review C*, 106(6):064004, 2022.

A Extended Related Works

In recent years, there has been considerable work on using machine learning methods to solve the static (time-independent) Schrödinger equation for many-body electronic systems. See the review article by [34] for an overview. These methods typically parametrize the ground state wave function ψ_θ using a neural network and optimize the parameters by minimizing the energy functional $\langle \psi_\theta, H \psi_\theta \rangle_{L^2}$. This framework has also been extended to the time-dependent Schrödinger equation for many-electron systems by [35]. This line of work is closely related to Physics-Informed Neural Networks (PINNs), which approximate solutions to PDEs by fitting a neural network ansatz that satisfies the variational form of the governing equations; see [36] and [37, Section 3.2.2.3]. However, these methods effectively act as solvers, requiring optimization for each new instance, and thus do not amortize computational costs. In contrast, our focus is on learning the global evolution operator directly from data, enabling fast and efficient evaluation for new initial conditions without retraining, thereby significantly reducing downstream computational cost.

An early work in learning solution operators for the Schrödinger equation was by [38], who trained a neural network to predict ground-state wave functions from potentials for the time-independent Schrödinger equation. More recently, [39] proposed an operator learning approach that models the solution operator mapping potentials to ground state wave functions by learning the associated Green's functions in a reproducing kernel Hilbert space (RKHS). A similar strategy was studied by [40], who used rotational neural networks to learn Green's functions for static Schrödinger equations. In addition, [40] also considered learning the green functions associated with time dependent propagator for 1-dimensional Harmonic oscillator.

A slightly more general framework was studied by [13], who used Fourier Neural Operators (FNOs) [17] to estimate the time evolution operator for simple quantum systems, such as random potentials and the double-slit potential. They also studied the ability of the learned operator to generalize across time, extrapolating beyond the training time range. Their learned operator is more flexible than ours in that it takes both the initial wave and the potential function as inputs, rather than assuming a fixed Hamiltonian. Relatedly, [22] studied learning the phases of amplitudes in scattering problems. Beyond isolated systems, [14] and [23] extended FNO-based architectures to model dissipative quantum systems that interact with an environment and are possibly driven by external fields, again evaluating time generalization. Most recently, [15] trained FNOs to learn the evolution operator for relatively larger quantum spin systems (up to 8-qubit systems), studying both single-step and multi-step time extrapolation.

We also note the related work on learning unitary transformations between large but finite-dimensional Hilbert spaces [41, 42, 43], a problem that has been studied extensively in areas ranging from quantum state simulation [44] to quantum computing [45]. Finally, there is a growing body of work on learning linear operators from data in the context of PDE modeling [46, 47, 27], which is most closely related to the perspective adopted in this work.

B Extensions to Non-Periodic Domains

Extending the results from Sections 3 and 5 to general *bounded* domain $\Omega \subset \mathbb{R}^d$ is straightforward. This requires choosing an orthonormal basis of $L^2(\Omega)$ and defining a corresponding Sobolev-type space. While any orthonormal basis of $L^2(\Omega)$ could be used, the most natural choice is the eigenfunctions of the Laplacian, which satisfy the eigenvalue problem,

$$-\Delta u = \lambda u, \quad \text{subject to appropriate boundary conditions.}$$

Common boundary conditions include Dirichlet, Neumann, and Robin.

For the special case $\Omega = \mathbb{T}^d$, the Laplacian eigenvalues are $\{4\pi^2|k|_2^2 : k \in \mathbb{Z}^d\}$, and the corresponding eigenfunctions are Fourier modes $\{\varphi_k\}_{k \in \mathbb{Z}^d}$. This motivates defining a more general Sobolev-type space using the eigenpairs of the Laplacian. Let $\{\lambda_j\}_{j=1}^\infty$ denote the eigenvalues such that $0 < \lambda_1 \leq \lambda_2 \leq \dots$, and let $\{\phi_j\}_{j=1}^\infty$ be the corresponding eigenfunctions. Then, the Sobolev-type space is defined as

$$\mathcal{H}^s(\Omega) = \left\{ f \in L^2(\Omega) \mid \sum_{j=1}^\infty (1 + |\lambda_j|)^s |\langle f, \phi_j \rangle_{L^2}|^2 < \infty \right\}.$$

For specific choices of Ω , this space might be defined more naturally using a weight function $\zeta(\lambda_j)^s$ for some function $\zeta : (0, \infty) \rightarrow (0, \infty)$, or by indexing the eigenvalues with another countable set, such as \mathbb{N}^d or \mathbb{Z}^d . Nevertheless, this general formulation captures the essential structure of the space. To avoid such indexing issue, one can define this space more implicitly as

$$\mathcal{H}^s(\Omega) := \left\{ f \in L^2(\Omega) \mid (\mathbf{I} - \Delta)^{s/2} f \in L^2(\Omega) \right\}.$$

The operator $(\mathbf{I} - \Delta)^{s/2}$ is called Bessel potential, and this space is also referred to as Bessel potential space. It is important to note that, unlike in the case of the torus, the equivalence between this Sobolev-type space and the classical Sobolev space defined using differential operators does not generally hold for arbitrary domains Ω . However, in applied operator learning, sample functions are typically generated using their spectral representation. Thus, we argue that the spectral definition of smoothness is arguably more natural from a practical perspective than the one based on differentials.

To construct the estimator from Section 3.1, given a sample budget of n , one queries the first n eigenfunctions $\phi_1, \phi_2, \dots, \phi_n$ instead of Fourier modes. The proofs then remain valid without modification, as they only rely on the fact that Fourier modes form an orthonormal basis of $L^2(\mathbb{T}^d)$. However, because the eigenvalues are indexed by \mathbb{N} in $\mathcal{H}^s(\Omega)$, the parameter s in this setting serves as an analog of s/d in $\mathcal{H}^s(\mathbb{T}^d)$.

In the experiments presented in Section 6, we also consider the case where Ω is a sphere and use spherical harmonics, which are the eigenfunctions of the Laplacian on a sphere. Similarly, Bessel functions serve as the Laplacian eigenfunctions in cylindrical domains. However, for general domains Ω , explicit eigenfunctions may not be available in closed form. In these cases, alternative bases such as orthonormal polynomials or wavelets, which are defined algebraically rather than through an eigenvalue problem, may be used. These bases form a complete system for sufficiently regular Ω' that contains Ω . A Sobolev-type space can then be defined using these algebraic bases and retain the theoretical guarantees established in this work.

B.1 Comparison to Function Generation in Applied Literature

Next, we discuss how our assumption that the initial wave ψ_0 lies in $\mathcal{H}^s(\Omega)$ is implicit in the function generation strategies commonly used in applied operator learning. In the applied literature, input functions are typically sampled from a Gaussian measure, $\mathcal{N}(0, (-\Delta + I)^{-\beta})$, or through some elementary push-forward of this distribution. This distribution, widely used in the applied stochastic PDE literature [48], was first introduced in the operator learning setting by [49] and has since been implemented in works such as [17, 16].

Let $(\lambda_j, \phi_j)_{j=1}^\infty$ be the eigenpairs of $-\Delta$ in Ω with the given boundary conditions. By the Spectral Mapping Theorem, the eigenvalues of the covariance operator $(-\Delta + I)^{-\beta}$ are $(\lambda_j + 1)^{-\beta}$, while the eigenfunctions remain ϕ_j 's. Applying the Karhunen-Loève Theorem [50, Theorem 7.3.5], a sample $u \sim \text{Normal}(0, (-\Delta + I)^{-\beta})$ drawn from this distribution has the decomposition

$$u(x) = \sum_{j=1}^{\infty} (\lambda_j + 1)^{-\beta/2} \xi_j \phi_j(x),$$

where $\{\xi_j\}_{j=1}^\infty$ are uncorrelated standard Gaussian random variables, meaning $\xi_j \sim \text{Normal}(0, 1)$ and $\mathbb{E}[\xi_i \xi_j] = \mathbb{1}[i = j]$. Thus, sampling u is reduced to generating a sequence of independent Gaussian random variables $(\xi_j)_{j=1}^\infty$. In practical implementations, this is done by truncating the sequence to $(\xi_j)_{j=1}^M$.

Using this decomposition, we compute

$$\mathbb{E}[|\langle u, \phi_j \rangle_{L^2}|^2] = (\lambda_j + 1)^{-\beta} \mathbb{E}[\xi_j^2] = (\lambda_j + 1)^{-\beta}.$$

Thus, for any $s > 0$, we have

$$\mathbb{E} \left[\sum_{j=1}^{\infty} (1 + \lambda_j)^s |\langle u, \phi_j \rangle_{L^2}|^2 \right] = \sum_{j=1}^{\infty} (1 + \lambda_j)^s (\lambda_j + 1)^{-\beta} = \sum_{j=1}^{\infty} (\lambda_j + 1)^{s-\beta}.$$

Recall that $\lambda_j \rightarrow \infty$ as $j \rightarrow \infty$. Thus, for large enough $\beta > 0$, there always exists $s < \beta$ such that $\sum_{j=1}^{\infty} (\lambda_j + 1)^{s-\beta} < \infty$. This shows that β controls the expected smoothness of samples from this distribution. More importantly, on average, these sampled functions belong to a Sobolev-type space. For a more detailed discussion of how β and s relate when $\Omega = \mathbb{T}^d$, we refer the reader to [27, Section B.1].

A similar strategy is used in [51], where functions are sampled from a Gaussian process with a covariance kernel given by the radial basis function (RBF) kernel, $k(x, y) = \exp\left(-\frac{\|x-y\|_2^2}{2\sigma^2}\right)$. Since the eigenvalues of the RBF kernel decay exponentially fast, a similar analysis shows that the sampled functions belong to an extremely smooth space, essentially corresponding to the limiting case $s = \infty$. This argument is not specific to the RBF kernel—any kernel with sufficiently fast eigenvalue decay produces functions with high regularity.

Therefore, the requirement that input wave functions ψ belong to a smooth space $\mathcal{H}^s(\Omega)$ is both reasonable and consistent with what is often an implicit assumption in applied operator learning literature.

C Proof of Proposition 3.1

Proof. Let $u, v \in L^2(\Omega)$. Expanding the inner product,

$$\begin{aligned} \langle \widehat{F}_n(u), \widehat{F}_n(v) \rangle_{L^2} &= \left\langle \sum_{|k|_\infty \leq K_n} w_k \langle u, \varphi_k \rangle_{L^2}, \sum_{|k|_\infty \leq K_n} w_k \langle v, \varphi_k \rangle_{L^2} \right\rangle_{L^2} \\ &= \sum_{|k|_\infty, |\ell|_\infty \leq K_n} \langle u, \varphi_k \rangle_{L^2} \overline{\langle v, \varphi_\ell \rangle_{L^2}} \langle w_k, w_\ell \rangle_{L^2}. \end{aligned}$$

Using the assumption on the PDE solver, we have

$$\langle w_k, w_\ell \rangle_{L^2} = \langle P(\varphi_k), P(\varphi_\ell) \rangle_{L^2} = \langle \varphi_k, \varphi_\ell \rangle_{L^2} = \mathbb{1}[k = \ell].$$

Substituting this into the sum,

$$\begin{aligned} \langle \widehat{F}_n(u), \widehat{F}_n(v) \rangle_{L^2} &= \sum_{|k|_\infty, |\ell|_\infty \leq K_n} \langle u, \varphi_k \rangle_{L^2} \overline{\langle v, \varphi_\ell \rangle_{L^2}} \mathbb{1}[k = \ell] \\ &= \sum_{|k|_\infty \leq K_n} \langle u, \varphi_k \rangle_{L^2} \overline{\langle v, \varphi_k \rangle_{L^2}}. \end{aligned}$$

Using Parseval's identity, we can rewrite this as

$$\begin{aligned} \sum_{|k|_\infty \leq K_n} \langle u, \varphi_k \rangle_{L^2} \overline{\langle v, \varphi_k \rangle_{L^2}} &= \sum_{k \in \mathbb{Z}^d} \langle u, \varphi_k \rangle_{L^2} \overline{\langle v, \varphi_k \rangle_{L^2}} - \sum_{|k|_\infty > K_n} \langle u, \varphi_k \rangle_{L^2} \overline{\langle v, \varphi_k \rangle_{L^2}} \\ &= \langle u, v \rangle_{L^2} - \sum_{|k|_\infty > K_n} \langle u, \varphi_k \rangle_{L^2} \overline{\langle v, \varphi_k \rangle_{L^2}}. \end{aligned}$$

Property (i) follows since the second summation vanishes when u, v belong to the span of $\{\varphi_k : k \in \mathbb{Z}^d, |k|_\infty \leq K_n\}$. To establish property (ii), setting $u = v$ in the above expression,

$$\|\widehat{F}_n(u)\|_{L^2}^2 = \|u\|_{L^2}^2 - \sum_{|k|_\infty > K_n} |\langle u, \varphi_k \rangle_{L^2}|^2 \leq \|u\|_{L^2}^2.$$

This completes the proof. \square

D Proof of Theorem 4.2

Proof. Recall that

$$\widehat{F}_n = \sum_{|k|_\infty \leq K_n} w_k \otimes \varphi_k.$$

For each k such that $|k|_\infty \leq K_n$, define the error term

$$\delta_k := w_k - F(\varphi_k).$$

By Assumption 4.1, it follows that $\|\delta_k\|_{L^2} \leq \varepsilon$. So, for any wave function $\psi \in \mathcal{H}^s(\mathbb{T}^d)$, we can expand

$$\begin{aligned} \widehat{F}_n(\psi) &= \sum_{|k|_\infty \leq K_n} w_k \langle \psi, \varphi_k \rangle_{L^2} \\ &= \sum_{|k|_\infty \leq K_n} F(\varphi_k) \langle \psi, \varphi_k \rangle_{L^2} + \sum_{|k|_\infty \leq K_n} \delta_k \langle \psi, \varphi_k \rangle_{L^2} \\ &= F \left(\sum_{|k|_\infty \leq K_n} \varphi_k \langle \psi, \varphi_k \rangle_{L^2} \right) + \sum_{|k|_\infty \leq K_n} \delta_k \langle \psi, \varphi_k \rangle_{L^2}, \end{aligned}$$

where the last equality follows from the linearity of F . Then, applying the triangle inequality,

$$\begin{aligned}
\|\widehat{F}_n(\psi) - F(\psi)\|_{L^2} &= \left\| F \left(\sum_{|k|_\infty \leq K_n} \varphi_k \langle \psi, \varphi_k \rangle_{L^2} \right) + \sum_{|k|_\infty \leq K_n} \delta_k \langle \psi, \varphi_k \rangle_{L^2} - F(\psi) \right\|_{L^2} \\
&= \left\| F \left(\sum_{|k|_\infty \leq K_n} \varphi_k \langle \psi, \varphi_k \rangle_{L^2} - \psi \right) + \sum_{|k|_\infty \leq K_n} \delta_k \langle \psi, \varphi_k \rangle_{L^2} \right\|_{L^2} \\
&\leq \left\| F \left(\sum_{|k|_\infty \leq K_n} \varphi_k \langle \psi, \varphi_k \rangle_{L^2} - \psi \right) \right\|_{L^2} + \left\| \sum_{|k|_\infty \leq K_n} \delta_k \langle \psi, \varphi_k \rangle_{L^2} \right\|_{L^2},
\end{aligned}$$

To bound the first term, note that the operator norm of F from a L^2 to L^2 is 1 as F is a unitary operator. So,

$$\begin{aligned}
\left\| F \left(\sum_{|k|_\infty \leq K_n} \varphi_k \langle \psi, \varphi_k \rangle_{L^2} - \psi \right) \right\|_{L^2} &\leq \left\| \sum_{|k|_\infty \leq K_n} \varphi_k \langle \psi, \varphi_k \rangle_{L^2} - \psi \right\|_{L^2} \\
&= \sqrt{\sum_{|k|_\infty > K_n} |\langle \psi, \varphi_k \rangle_{L^2}|^2} \\
&= \sqrt{\sum_{|k|_\infty > K_n} \frac{(1 + |k|_2^2)^s}{(1 + |k|_2^2)^s} |\langle \psi, \varphi_k \rangle_{L^2}|^2} \\
&\leq \sqrt{\frac{1}{(1 + K_n^2)^s}} \sqrt{\sum_{|k|_\infty > K_n} (1 + |k|_2^2)^s |\langle \psi, \varphi_k \rangle_{L^2}|^2} \\
&\leq K_n^{-s} \|\psi\|_{\mathcal{H}^s}.
\end{aligned}$$

The first equality follows from Parseval's identity.

To bound the contribution from the PDE solver error, we use triangle inequality to get

$$\begin{aligned}
\left\| \sum_{|k|_\infty \leq K_n} \delta_k \langle \psi, \varphi_k \rangle_{L^2} \right\|_{L^2} &\leq \sum_{|k|_\infty \leq K_n} \|\delta_k\|_{L^2} |\langle \psi, \varphi_k \rangle_{L^2}| \\
&\leq \varepsilon \sum_{|k|_\infty \leq K_n} |\langle \psi, \varphi_k \rangle_{L^2}| \\
&\leq \varepsilon \sum_{|k|_\infty \leq K_n} \sqrt{\frac{(1 + |k|_2^2)^s}{(1 + |k|_2^2)^s}} |\langle \psi, \varphi_k \rangle_{L^2}| \\
&\leq \varepsilon \sqrt{\sum_{|k|_\infty \leq K_n} \frac{1}{(1 + |k|_2^2)^s}} \sqrt{\sum_{|k|_\infty \leq K_n} (1 + |k|_2^2)^s |\langle \psi, \varphi_k \rangle_{L^2}|^2} \\
&\leq \varepsilon \|\psi\|_{\mathcal{H}^s} \sqrt{\sum_{|k|_\infty \leq K_n} \frac{1}{(1 + |k|_2^2)^s}} \\
&= \varepsilon \|\psi\|_{\mathcal{H}^s} \gamma_n,
\end{aligned}$$

where

$$\gamma_n := \sqrt{\sum_{|k|_\infty \leq K_n} \frac{1}{(1 + |k|_2^2)^s}}.$$

Thus, we have established that

$$\|\widehat{F}_n(\psi) - F(\psi)\|_{L^2} \leq \|\psi\|_{\mathcal{H}^s} (\varepsilon \gamma_n + K_n^{-s}).$$

Note that $K_n = (n^{1/d} - 1)/2 \geq n^{1/d}/3$ as long as $n \geq 3^d$. This yields that $K_n^{-s} \leq 3^s n^{-s/d}$.

To bound γ_n , recall that $|\{k \in \mathbb{Z}^d : |k|_\infty = j\}| = 2(2j+1)^{d-1}$. This is because one of the entry of m has to be $\pm j$ and other $d-1$ entries could be anything in $\{-j, \dots, -1, 0, 1, \dots, j\}$. Thus,

$$\begin{aligned} \gamma_n^2 &= \sum_{|k|_\infty \leq K_n} \frac{1}{(1 + |k|_2^2)^s} \leq \sum_{|k|_\infty \leq K_n} \frac{1}{(1 + |k|_\infty^2)^s} \leq 1 + \sum_{1 < |k|_\infty \leq K_n} \frac{1}{(1 + |k|_\infty^2)^s} \\ &\leq 1 + \sum_{j=1}^{K_n} \frac{2(2j+1)^{d-1}}{(1 + j^2)^s} \\ &\leq 1 + \sum_{j=1}^{K_n} \frac{2(2j+1)^{d-1}}{j^{2s}} \\ &\leq 1 + 2 \cdot 3^{d-1} \sum_{j=1}^{K_n} \frac{1}{j^{2s-d+1}} \\ &\lesssim \int_1^{K_n} \frac{1}{t^{2s-d+1}} dt \\ &\lesssim \begin{cases} 1, & \text{if } 2s > d, \\ \log(K_n), & \text{if } 2s = d, \\ K_n^{d-2s} & \text{if } 2s < d. \end{cases} \end{aligned}$$

Our proof completes upon noting that $K_n \lesssim n^{1/d}$. □

E Proof of Theorem 4.3

Proof. We will break down the proof into multiple steps.

Defining the Hamiltonian: Considering the case where the potential is zero, meaning $V(x) = 0$ for all $x \in \mathbb{T}^d$. In this case, the Hamiltonian simplifies to

$$H = -\frac{\hbar^2}{2m} \Delta.$$

The corresponding solution operator is given by

$$F = \exp\left(-\frac{i}{\hbar} T H\right) = \exp\left(i \frac{\hbar T}{2m} \Delta\right).$$

Note that the Fourier modes are eigenfunctions of this operator. Specifically, for any wave vector k , we have

$$F(\varphi_k) = \exp\left(-i \frac{4\pi^2 |k|_2^2 \hbar T}{2m}\right) \varphi_k.$$

This follows from expanding the operator exponential and using the property

$$\Delta \varphi_k = \sum_{j=1}^d \frac{\partial^2 e^{2\pi i k \cdot x}}{\partial x_j^2} = \sum_{j=1}^d (2\pi i)^2 k_j^2 e^{2\pi i k \cdot x} = -4\pi^2 |k|_2^2 \varphi_k.$$

Defining

$$\eta_k := \exp\left(-i \frac{4\pi^2 |k|_2^2 \hbar T}{2m}\right),$$

we can express the action of the solution operator as

$$F(\varphi_k) = \eta_k \varphi_k.$$

Specifying a PDE Solver. Our next step is to specify the exact details of the PDE solver that satisfies the ε -approximate assumption while also allowing us to construct hard instances to establish the lower bound. To that end, let P be the PDE solver defined as

$$P(u) = F(u) + \varepsilon \varphi_0, \quad \text{for every } u \in L^2(\Omega).$$

Here, φ_0 is simply the constant function 1 on the domain. That is, our PDE solver oracle returns the true solution shifted by $\varepsilon \varphi_0$ noise. While such a PDE solver is not practical, it is still a valid ε -approximate oracle since $\|\varphi_0\|_{L^2} = 1$, and thus our upper bound in Theorem 4.2 applies.

Writing out the Estimator. For this solution operator and the PDE solver specified above, our estimator has a more concrete form. In particular, we can write

$$\hat{F} := \sum_{|k|_\infty \leq K_n} \eta_k \varphi_k \otimes \varphi_k + \varepsilon \sum_{|k|_\infty \leq K_n} \varphi_0 \otimes \varphi_k.$$

Defining the Test Function. Given a sample size budget of n , we now construct a hard test wave function ψ_{test} to establish the claimed lower bound. To do this, choose a large $M \gg n$, which will be specified later, and define ψ_{test} as

$$\psi_{\text{test}} = \sum_{|k|_\infty \leq M} c_k \varphi_k,$$

for some coefficients $c_k \geq 0$.

Establishing the Lower Bound. For the wave function ψ_{test} defined above, the true evolution under F is given by

$$F(\psi_{\text{test}}) = \sum_{|k|_\infty \leq M} c_k \eta_k \varphi_k.$$

On the other hand, the estimator \hat{F}_n produces

$$\hat{F}_n(\psi_{\text{test}}) = \sum_{|k|_\infty \leq K_n} c_k \eta_k \varphi_k + \varepsilon \sum_{|k|_\infty \leq K_n} c_k \varphi_0.$$

Rewriting the second term,

$$\hat{F}_n(\psi_{\text{test}}) = \sum_{|k|_\infty \leq K_n} c_k \eta_k \varphi_k + \varepsilon \left(\sum_{|k|_\infty \leq K_n} c_k \right) \varphi_0.$$

Thus, the difference between the estimated and true evolution is

$$\hat{F}_n(\psi_{\text{test}}) - F(\psi_{\text{test}}) = \varepsilon \left(\sum_{|k|_\infty \leq K_n} c_k \right) \varphi_0 - \sum_{K_n < |k|_\infty \leq M} c_k \eta_k \varphi_k.$$

Using Parseval's identity, we obtain

$$\begin{aligned} \left\| \hat{F}_n(\psi_{\text{test}}) - F(\psi_{\text{test}}) \right\|_{L^2}^2 &= \varepsilon^2 \left| \sum_{|k|_\infty \leq K_n} c_k \right|^2 + \sum_{K_n < |k|_\infty \leq M} |c_k \eta_k|^2 \\ &= \varepsilon^2 \sum_{|k|_\infty \leq K_n} |c_k|^2 + \sum_{K_n < |k|_\infty \leq M} |c_k|^2, \end{aligned}$$

where the last step follows from the assumptions that $c_k \geq 0$ and $|\eta_k| = 1$ for all $k \in \mathbb{Z}^d$. To establish the claimed rate, we now choose c_k appropriately while ensuring that $\|\psi_{\text{test}}\| = 1$ and $\|\psi_{\text{test}}\|_{\mathcal{H}^s} \leq 2$. To that end, we fix an index ℓ such that $|\ell|_\infty = \lceil K_n + 1 \rceil$ and set

$$c_\ell = \frac{1}{(1 + |\ell|_2^2)^{s/2}}.$$

This ensures that

$$\sum_{K_n < |k|_\infty \leq M} |c_k|^2 \geq |c_\ell|^2 = \frac{1}{(1 + |\ell|_2^2)^s} \gtrsim \frac{1}{K_n^{2s}} \gtrsim \frac{1}{n^{2s/d}}.$$

It now remains to bound $\sum_{|k|_\infty \leq K_n} |c_k|$, for which we proceed with a case analysis.

Case (I): $s \geq d/2$. In this case, we can simply set

$$c_0 := \sqrt{1 - c_\ell^2}$$

and assign $c_k = 0$ for all $k \notin \{0, \ell\}$. It is straightforward to verify that

$$\|\psi_{\text{test}}\|_{L^2}^2 = (1 - c_\ell^2) + c_\ell^2 = 1,$$

and

$$\|\psi_{\text{test}}\|_{\mathcal{H}^s}^2 = c_0^2 + (1 + |\ell|_2^2)^s c_\ell^2 = 1 - c_\ell^2 + 1 \leq 2.$$

Thus, we obtain

$$\sum_{|k|_\infty \leq K_n} |c_k| \geq |c_0| = \sqrt{1 - c_\ell^2} \geq \frac{1}{\sqrt{2}},$$

since $c_\ell \leq 1/2$ for sufficiently large K_n .

Case (II): $s < d/2$. Define

$$R_n := \sum_{0 < |k|_\infty \leq K_n} 1.$$

Now, set

$$c_k := \sqrt{\frac{1}{R_n(1 + K_n^{2s})}}$$

for all $0 < |k|_\infty \leq K_n$, and let $c_k = 0$ for all $|k|_\infty > K_n$ such that $k \neq \ell$. It follows that

$$\begin{aligned} \|\psi_{\text{test}}\|_{L^2}^2 &= |c_0|^2 + \sum_{|k|_\infty \leq K_n} \frac{1}{R_n(1 + K_n^{2s})} + \frac{1}{(1 + |\ell|_2^2)^s} \\ &= |c_0|^2 + \frac{1}{(1 + K_n^{2s})} + \frac{1}{(1 + \lceil K_n + 1 \rceil_2^2)^s}. \end{aligned}$$

For sufficiently large n , the second and third terms can each be made at most $1/3$, allowing $1 \geq c_0 > 0$ to be chosen appropriately so that $\|\psi_{\text{test}}\|_{L^2} = 1$ and ψ_{test} is a valid wave function.

Next, note that

$$\begin{aligned} \|\psi_{\text{test}}\|_{\mathcal{H}^s}^2 &= |c_0|^2 + \sum_{0 < |k|_\infty \leq K_n} \frac{(1 + |k|_2^2)^s}{R_n(1 + K_n^{2s})} + (1 + |\ell|_2^2)^s c_\ell^2 \\ &\leq |c_0|^2 + \sum_{0 < |k|_\infty \leq K_n} \frac{1}{R_n} + 1 \\ &\leq 3. \end{aligned}$$

Thus, the sum is

$$\sum_{|k|_\infty \leq K_n} |c_k| \geq \sum_{0 < |k|_\infty \leq K_n} \sqrt{\frac{1}{R_n(1+K_n^2)^s}} = \sqrt{\frac{1}{R_n(1+K_n^2)^s}} \cdot R_n = \sqrt{\frac{R_n}{(1+K_n^2)^s}}.$$

Since $R_n \gtrsim K_n^d$, we obtain

$$\sum_{|k|_\infty \leq K_n} |c_k| \gtrsim \sqrt{K_n^{d-2s}} \gtrsim \sqrt{n^{1-\frac{2s}{d}}} = n^{\frac{1}{2}-\frac{s}{d}}.$$

Thus, we have established the lower bound of

$$\gtrsim \begin{cases} \varepsilon^2 + n^{-2s/d}, & \text{if } 2s \geq d, \\ \varepsilon^2 n^{\frac{1}{2}-\frac{s}{d}} + n^{-2s/d} & \text{if } 2s < d. \end{cases}$$

However, this is a lower bound for the squared norm. Using the inequality $\sqrt{a^2 + b^2} \geq \frac{1}{\sqrt{2}}(|a| + |b|)$ completes our proof. \square

F Refined Upper Bound Under Stronger Assumptions on PDE Solver.

From the proof of the lower bound in Appendix E, it is evident that establishing Theorem 4.3 relies on a somewhat unnatural and almost adversarial PDE solver. This raises the question of whether a tighter bound can be achieved for more realistic, non-adversarial PDE solvers. A natural way to model such solvers is to assume that their errors behave as uncorrelated random noise.

Assumption F.1. For the Fourier modes φ_k , assume that the PDE solver satisfies $P(\varphi_k) = F(\varphi_k) + \delta_k$, where δ_k is a random variable in $L^2(\mathbb{T}^d)$ such that: (i) $\mathbb{E}[\|\delta_k\|_{L^2}^2] \leq \varepsilon^2$ and (ii) $\mathbb{E}[\langle \delta_k, \delta_\ell \rangle_{L^2}] = 0$ for all $k \neq \ell$.

This assumption effectively places the problem as the fixed-design regression under uncorrelated, homoscedastic noise—a well-studied model in statistics. However, unlike in classical statistics, where the learner is given a fixed design matrix, our setting allows the learner to actively choose the design matrix. Under this stronger assumption on the solver, we establish the following improved upper bound on the estimator.

Theorem F.2 (Improved Upper Bound). *Under Assumption F.1, the estimator defined in Equation (1) satisfies*

$$\mathbb{E} \left[\sup_{\|\psi\|_{\mathcal{H}^s} \leq c} \|\hat{F}_n(\psi) - F(\psi)\|_{L^2} \right] \leq \varepsilon + 3^s c n^{-\frac{s}{d}}.$$

Here, the expectation is taken over the randomness introduced by the δ_k 's in the estimator. Notably, the expectation is applied *after* the supremum over all wave functions in the Sobolev ball of radius c . This ensures that we are still bounding the error uniformly rather than in the mean-squared sense as is common in statistical learning theory. The expectation is required only because the uniform error is now a random variable. We defer the proof of Theorem F.2 to Appendix F. Lastly, we want to point out that a straightforward adaptation of the proof of Theorem F.2 can improve this result to a high-probability bound, provided the tails of δ_k 's decay sufficiently fast. In particular, assuming that δ_k 's are subgaussian in $L^2(\mathbb{T}^d)$ is sufficient for this improvement.

Proof of Theorem F.2. Our proof here largely follow the proof of Theorem 4.2 provided in Appendix D. Recall that, for any wave function ψ , we established in the proof of Theorem 4.2 that

$$\|\hat{F}_n(\psi) - F(\psi)\|_{L^2} \leq \left\| F \left(\sum_{|k|_\infty \leq K_n} \varphi_k \langle \psi, \varphi_k \rangle_{L^2} - \psi \right) \right\|_{L^2} + \left\| \sum_{|k|_\infty \leq K_n} \delta_k \langle \psi, \varphi_k \rangle_{L^2} \right\|_{L^2}.$$

The first term does not have any randomness. So, following the same argument as in that proof, we can show that

$$\left\| F \left(\sum_{|k|_\infty \leq K_n} \varphi_k \langle \psi, \varphi_k \rangle_{L^2} - \psi \right) \right\|_{L^2} \leq K_n^{-s} \|\psi\|_{\mathcal{H}^s} \leq 3^s c n^{-\frac{s}{d}}.$$

Here, we used the definition of K_n and the fact that $\|\psi\|_{\mathcal{H}^s} \leq c$. Now, it remains to bound the term with δ_k 's. Since this is a random variable, we want to bound its expectation. To that end, Jensen's inequality implies

$$\mathbb{E} \left[\left\| \sum_{|k|_\infty \leq K_n} \delta_k \langle \psi, \varphi_k \rangle_{L^2} \right\|_{L^2}^2 \right] \leq \sqrt{\mathbb{E} \left[\left\| \sum_{|k|_\infty \leq K_n} \delta_k \langle \psi, \varphi_k \rangle_{L^2} \right\|_{L^2}^4 \right]}.$$

Note that

$$\begin{aligned} \left\| \sum_{|k|_\infty \leq K_n} \delta_k \langle \psi, \varphi_k \rangle_{L^2} \right\|_{L^2}^2 &= \left\langle \sum_{|k|_\infty \leq K_n} \delta_k \langle \psi, \varphi_k \rangle_{L^2}, \sum_{|k|_\infty \leq K_n} \delta_k \langle \psi, \varphi_k \rangle_{L^2} \right\rangle_{L^2} \\ &= \sum_{|k|_\infty, |\ell|_\infty \leq K_n} \langle \psi, \varphi_k \rangle_{L^2} \overline{\langle \psi, \varphi_\ell \rangle_{L^2}} \langle \delta_k, \delta_\ell \rangle_{L^2} \\ &= \sum_{|k|_\infty \leq K_n} |\langle \psi, \varphi_k \rangle_{L^2}|^2 \|\delta_k\|_{L^2}^2 + \sum_{k \neq \ell} \langle \psi, \varphi_k \rangle_{L^2} \overline{\langle \psi, \varphi_\ell \rangle_{L^2}} \langle \delta_k, \delta_\ell \rangle_{L^2} \end{aligned}$$

Note that the cross terms $k \neq \ell$ vanishes in expectation due to part (ii) of Assumption F.1. Using part (i) of Assumption F.1 yields

$$\begin{aligned} \mathbb{E} \left[\left\| \sum_{|k|_\infty \leq K_n} \delta_k \langle \psi, \varphi_k \rangle_{L^2} \right\|_{L^2}^2 \right] &= \sum_{|k|_\infty \leq K_n} |\langle \psi, \varphi_k \rangle_{L^2}|^2 \mathbb{E}[\|\delta_k\|_{L^2}^2] \\ &\leq \varepsilon^2 \sum_{|k|_\infty \leq K_n} \langle \psi, \varphi_k \rangle_{L^2} \\ &\leq \varepsilon^2, \end{aligned}$$

where the final step uses the fact that $\|\psi\|_{L^2}^2 = 1$. This shows that

$$\mathbb{E} \left[\left\| \sum_{|k|_\infty \leq K_n} \delta_k \langle \psi, \varphi_k \rangle_{L^2} \right\|_{L^2} \right] \leq \varepsilon.$$

This completes our proof. □

G Proof of Theorem 5.1

Proof. Note that

$$\widehat{\mathbf{F}}_n^q \psi - \mathbf{F}^q \psi = (\widehat{\mathbf{F}}_n^q - \mathbf{F}^q) \psi = \sum_{j=0}^{q-1} \widehat{\mathbf{F}}_n^{q-1-j} (\widehat{\mathbf{F}}_n - \mathbf{F}) \mathbf{F}^j \psi.$$

Applying the triangle inequality,

$$\|\widehat{\mathbf{F}}_n^q \psi - \mathbf{F}^q \psi\|_{L^2} \leq \sum_{j=0}^{q-1} \left\| \widehat{\mathbf{F}}_n^{q-1-j} (\widehat{\mathbf{F}}_n - \mathbf{F}) \mathbf{F}^j \psi \right\|_{L^2}.$$

Using property (ii) of Proposition 3.1 iteratively $q - j - 1$ times, we obtain

$$\left\| \widehat{\mathbf{F}}_n^{q-1-j} (\widehat{\mathbf{F}}_n - \mathbf{F}) \mathbf{F}^j \psi \right\|_{L^2} \leq \left\| (\widehat{\mathbf{F}}_n - \mathbf{F}) \mathbf{F}^j \psi \right\|_{L^2}.$$

Furthermore, applying Theorem 4.2, we obtain the bound

$$\left\| (\widehat{F}_n - F) F^j \psi \right\|_{L^2} \leq \|F^j \psi\|_{\mathcal{H}^s} \left(\varepsilon \gamma_n + 3^s n^{-s/d} \right).$$

Thus, we conclude that

$$\|\widehat{F}_n^q \psi - F^q \psi\|_{L^2} \leq \left(\varepsilon \gamma_n + 3^s n^{-s/d} \right) \sum_{j=0}^{q-1} \|F^j \psi\|_{\mathcal{H}^s}.$$

□

H Proof of Corollary 5.2

H.1 Proof of Part (i)

Proof. Let $V(x) = a$ for all $x \in \mathbb{T}^d$. Then, for every Fourier mode φ_k , the Hamiltonian acts as

$$H \varphi_k = \left(-\frac{\hbar^2}{2m} \Delta + V(\cdot) \right) \varphi_k = \left(\frac{\hbar^2}{2m} 4\pi^2 |k|_2^2 + a \right) \varphi_k.$$

The second equality holds because φ_k is an eigenfunction of $-\Delta$ with eigenvalue $4\pi^2 |k|_2^2$. Next, applying the time evolution operator, we get

$$F(\varphi_k) = e^{-\frac{i}{\hbar} T H} \varphi_k = e^{-\frac{i}{\hbar} T \left(\frac{\hbar^2}{2m} 4\pi^2 |k|_2^2 + a \right)} \varphi_k.$$

Since the modulus of the complex exponential factor is always one, we can use this identity to establish that

$$\begin{aligned} \|F(\psi)\|_{\mathcal{H}^s} &= \sqrt{\sum_{k \in \mathbb{Z}^d} (1 + |k|_2^2)^s |\langle F(\psi), \varphi_k \rangle_{L^2}|^2} \\ &= \sqrt{\sum_{k \in \mathbb{Z}^d} (1 + |k|_2^2)^s \left| \left\langle \sum_{\ell \in \mathbb{Z}^d} \langle \psi, \varphi_\ell \rangle F(\varphi_\ell), \varphi_k \right\rangle_{L^2} \right|^2} \\ &= \sqrt{\sum_{k \in \mathbb{Z}^d} (1 + |k|_2^2)^s \left| \left\langle \sum_{\ell \in \mathbb{Z}^d} \langle \psi, \varphi_\ell \rangle e^{-\frac{i}{\hbar} T \left(\frac{\hbar^2}{2m} 4\pi^2 |\ell|_2^2 + a \right)} \varphi_\ell, \varphi_k \right\rangle_{L^2} \right|^2} \\ &= \sqrt{\sum_{k \in \mathbb{Z}^d} (1 + |k|_2^2)^s |\langle \psi, \varphi_k \rangle|^2}, \end{aligned}$$

where the final equality uses the fact that $\langle \varphi_\ell, \varphi_k \rangle = \mathbb{1}[k = \ell]$ and $\left| e^{-\frac{i}{\hbar} T \left(\frac{\hbar^2}{2m} 4\pi^2 |k|_2^2 + a \right)} \right| = 1$. Applying this iteratively for j steps, we obtain $\|F^j(\psi)\|_{\mathcal{H}^s} = \|\psi\|_{\mathcal{H}^s}$ for all $j \in \mathbb{N}$. □

H.2 Proof Part (ii)

Proof. Our result follows directly from the bound in [52, Theorem 1], originally established by [28], which states that

$$\|F^j \psi\|_{\mathcal{H}^s} = \|\psi(\cdot, jT)\|_{\mathcal{H}^s} \leq c(1 + jT) \|\psi\|_{\mathcal{H}^s}.$$

This can be further refined using [52, Equation 1.3], yielding the bound

$$\|F^j \psi\|_{\mathcal{H}^s} \leq c(1 + jT)^\varepsilon \|\psi\|_{\mathcal{H}^s}$$

for any fixed $\varepsilon > 0$. Substituting this into our generalization bound gives

$$\left\| \widehat{F}_n^q(\psi) - F^q(\psi) \right\|_{L^2} \leq \|\psi\|_{\mathcal{H}^s} \left(\varepsilon \gamma_n + 3^s n^{-s/d} \right) \cdot c q(1 + Tq)^\varepsilon.$$

□

H.3 Proof Part (iii)

Proof. Since the Hamiltonian H is time-independent, the evolution operator satisfies

$$F^j \psi = e^{-ijTH/\hbar} \psi.$$

Defining $\psi(t)$ as the wave function at time t with initial condition $\psi(0) = \psi$, we write

$$F^j \psi = \psi(jT).$$

Thus, bounding the Sobolev norm of $F^j \psi$ reduces to bounding $\|\psi(t)\|_{\mathcal{H}^s}$ in terms of $\|\psi(0)\|_{\mathcal{H}^s}$ for all $t > 0$. To proceed, define the operator

$$\Lambda^s := (I - (4\pi^2)^{-1} \Delta)^{s/2}.$$

Note that

$$\begin{aligned} \|\Lambda^s \psi\|_{L^2}^2 &= \left\| \sum_{k \in \mathbb{Z}^d} \langle \psi, \varphi_k \rangle_{L^2} \Lambda^s \varphi_k \right\|_{L^2}^2 = \left\| \sum_{k \in \mathbb{Z}^d} \langle \psi, \varphi_k \rangle_{L^2} (1 + |k|_2^2)^{s/2} \varphi_k \right\|_{L^2}^2 \\ &= \sum_{k \in \mathbb{Z}^d} (1 + |k|_2^2)^s |\langle \psi, \varphi_k \rangle_{L^2}|^2 \\ &= \|\psi\|_{\mathcal{H}^s}^2. \end{aligned}$$

Thus, we focus on bounding $\|\Lambda^s \psi(t)\|_{L^2}$.

Energy Functional. Define the energy functional

$$E_s(t) := \|\Lambda^s \psi(t)\|_{L^2}^2.$$

Using the product rule rule in a Hilbert space, we obtain

$$\frac{d}{dt} E_s(t) = \langle \Lambda^s(\partial_t \psi), \Lambda^s \psi \rangle_{L^2} + \langle \Lambda^s \psi, \Lambda^s(\partial_t \psi) \rangle_{L^2} = 2 \operatorname{Re} (\langle \Lambda^s(\partial_t \psi), \Lambda^s \psi \rangle_{L^2}).$$

Since the Schrödinger equation states

$$\partial_t \psi = i \frac{\hbar}{2m} \Delta \psi - \frac{i}{\hbar} V \psi,$$

applying Λ^s to both sides yields

$$\Lambda^s(\partial_t \psi) = i \frac{\hbar}{2m} \Lambda^s(\Delta \psi) - \frac{i}{\hbar} \Lambda^s(V \psi).$$

Thus, we obtain the energy functional equation

$$\frac{d}{dt} E_s(t) = 2 \operatorname{Re} \left(\left\langle i \frac{\hbar}{2m} \Lambda^s(\Delta \psi) - \frac{i}{\hbar} \Lambda^s(V \psi), \Lambda^s \psi \right\rangle_{L^2} \right).$$

Note that

$$\operatorname{Re} \left\langle i \frac{\hbar}{2m} \Lambda^s(\Delta \psi), \Lambda^s \psi \right\rangle = \operatorname{Re} \left(i \frac{\hbar}{2m} \langle \Lambda^s(\Delta \psi), \Lambda^s \psi \rangle \right) = 0.$$

This follows because $\langle \Lambda^s(\Delta \psi), \Lambda^s \psi \rangle$ is a real number. To see why, observe that we can rewrite

$$\langle \Lambda^s(\Delta \psi), \Lambda^s \psi \rangle = \langle (\Lambda^s \Delta \Lambda^{-s}) \Lambda^s \psi, \Lambda^s \psi \rangle.$$

Since $(\Lambda^s \Delta \Lambda^{-s})$ is a self-adjoint operator on L^2 , the inner product must be real. So, the only contribution comes from

$$-\frac{i}{\hbar} \Lambda^s(V \psi).$$

Thus, we obtain

$$\frac{d}{dt} E_s(t) = -\frac{2}{\hbar} \operatorname{Im} \langle \Lambda^s(V \psi), \Lambda^s \psi \rangle_{L^2}.$$

Applying the Cauchy–Schwarz inequality,

$$\left| \frac{d}{dt} E_s(t) \right| \leq \frac{2}{\hbar} \|\Lambda^s(V \psi)\|_{L^2} \|\Lambda^s \psi\|_{L^2} = \frac{2}{\hbar} \|\Lambda^s(V \psi)\|_{L^2} \sqrt{E_s(t)}.$$

Bounding the Sobolev Norm of $V\psi$. By assumption, V belongs to $\mathcal{H}^r(\mathbb{T}^d)$. We will now establish

$$\|V\psi\|_{\mathcal{H}^s} \leq a\|V\|_{\mathcal{H}^r}\|\psi\|_{\mathcal{H}^s}$$

for some universal $a > 0$ that only depends on s, d, r . This is a Hölder-type inequality for the Sobolev norm of a product of two functions, commonly known as a Sobolev multiplication inequality. This inequality is established in the proof of [53, Theorem 5.1] for the domain \mathbb{R}^d (take $p_1 = p_2 = p = 2$, $s_1 = r$, and $s_2 = s$). The proof works verbatim for \mathbb{T}^d as it only uses the Sobolev Embedding Theorems, which continue to hold on \mathbb{T}^d .

Thus, rewriting in terms of Λ^s yields

$$\|\Lambda^s(V\psi)\|_{L^2} \leq a\|V\|_{\mathcal{H}^r}\|\psi\|_{\mathcal{H}^s},$$

which upon using the definition of energy functional implies

$$\|\Lambda^s(V\psi)\|_{L^2} \leq a\|V\|_{\mathcal{H}^r}\sqrt{E_s(t)}.$$

Applying Grönwall's Inequality. Substituting this inequality into our bound for $\frac{d}{dt}E_s(t)$, we obtain

$$\left| \frac{d}{dt}E_s(t) \right| \leq \frac{2a}{\hbar}\|V\|_{\mathcal{H}^r}E_s(t).$$

Applying Grönwall's inequality on $[0, t]$, we obtain

$$E_s(t) \leq E_s(0) \exp\left(\frac{2a}{\hbar}\|V\|_{\mathcal{H}^r} \cdot t\right).$$

Finally, using the equivalence of norms,

$$\|\psi(t)\|_{\mathcal{H}^s}^2 \leq \|\psi(0)\|_{\mathcal{H}^s}^2 \exp\left(\frac{2a}{\hbar}\|V\|_{\mathcal{H}^r} \cdot t\right).$$

Taking square roots on both sides and defining $c := \frac{2a}{\hbar}$, we conclude

$$\|\psi(t)\|_{\mathcal{H}^s} \leq \|\psi(0)\|_{\mathcal{H}^s} \exp(c\|V\|_{\mathcal{H}^r} \cdot t).$$

□

I Experimental Potentials Details

We here provided more detailed descriptions of the potentials studied in the main text.

Free Particle If a particle is not exposed to an external potential, $V(x) = 0$ for all $x \in \Omega$.

Harmonic Oscillator Molecular vibrations are naturally modeled with a potential $V(x) = \frac{1}{2}m\omega^2|x|_2^2$, where m is the particle mass and ω the angular frequency of the oscillation.

Double Slit For a particle traveling across a barrier of potential V_0 at $x = x_0$ with two slits centered at y_1 and y_2 each with width w that are sufficiently far apart such that $|y_1 - y_2| \gg w$, the system potential is given by $V(x, y) = V_0$ when $x = x_0$ and $|y - y_1| > \frac{w}{2}$ and $|y - y_2| > \frac{w}{2}$, whereas $V(x, y) = 0$ otherwise.

Random Potentials To demonstrate robustness over arbitrary smooth potentials, a random potential $V(x)$ was drawn from a Gaussian Random Field identically to how such draws were made to define initial conditions, with $\alpha = 1$, $\beta = 1$, and $\gamma = 4$.

Coloumb Potential For a particle exposed to a radially symmetric electric field, such as in a Hydrogen atom, the potential is given by $V(x) = -\frac{ke^2}{r^2}$. We specifically focus on the case of a fixed radius of $r = 1$, for which the system can be modeled as a uniform field in spherical coordinates. As discussed, both the pseudospectral solver and estimator were computed using spherical harmonics for this setup.

Paul Trap for Qubit Design A Paul trap is a device that confines charged particles, such as ions, using oscillating electric fields. Notably, therefore, such a potential is time-dependent. For a detailed mathematical treatment of the Paul trap, see [54, Chapter 2]. A broader discussion on how Paul traps are used to localize charged ions for qubit encoding in their energy states can be found in the review article by [55]. In 2D, the potential function is given by $V(x, y, t) = \frac{U_0 + V_0 \cos(\omega t)}{r_0^2}(x^2 + y^2)$.

Shaken Lattice Optical lattices are a common design pattern for trapping neutral atoms with laser interferometry [56]. The promise in certain applications, such as quantum computing, is subsequent manipulation of such trapped atoms [57]. One mechanism of control is known as “shaking,” in which the phase of the potentials is manipulated to affect the momenta of the trapped particles [58, 59, 60]. If the shaking is restricted to a single axis, the potential is then given by $V(x, y, t) = V_0 \cos[k(x - A \sin(\omega t))] + V_0 \cos(ky)$.

Pulsed Gaussian Recent works have begun investigating the stability of bound states under pulsed external potentials, such as that of deuterons as studied in [61]. In particular, stability was assessed in the presence of external Gaussian pulses, given by the potential $V(x, y, t) = V_0 \exp\left(-\frac{(x-x_0)^2}{2\sigma_x^2} - \frac{(y-y_0)^2}{2\sigma_y^2}\right) \sum_{t_0} e^{-\frac{(t-t_0)^2}{2\sigma_t^2}}$.

We further provide the choices of parameters used for the experiments in Table 4.

Table 4: Parameter values used in the implementation of each potential.

Potential Name	Parameter Values
Free Particle	—
Barrier	$V_0 = 50.0, w = 0.2$
Harmonic Oscillator	$m = 1.0, \omega = 2.0$
Random Field (GRF)	$\alpha = 1, \beta = 1, \gamma = 4$
Paul Trap	$U_0 = 10.0, V_0 = 15.0, \omega = 3.0, r_0 = 2.0$
Shaken Lattice	$V_0 = 4.0, k_{\text{lat}} = 4\pi, A = 0.08, \omega_{\text{sh}} = 15.0$
Gaussian Pulse	$V = 100.0, x_0 = 0.0, y_0 = 0.0, \sigma_x = \sigma_y = 1.2,$ $\sigma_t = 1.0, t_{\text{centers}} = \{0.0\}$
Coulomb	$k = 1.0, e = 1.0$
Coulomb Dipole	$V_0 = 1.0$

J Additional Experimental Results

We present in Table 5 the results for the case where the test functions have a spectrum to match that of the linear estimator, i.e. where $|k|_\infty \leq K_n$.

Table 5: Average relative errors across Hamiltonians assessed over a batch of 100 i.i.d. test samples with a restricted spectrum. p-values for the hypothesis test $H_A : \mathcal{V}_{\text{err}}^{(\text{lin})} < \mathcal{V}_{\text{err}}^{(\text{FNO})}$ are also provided.

	FNO	DeepONet	Linear	$\mathcal{V}_{\text{err}}^{(\text{lin})} < \mathcal{V}_{\text{err}}^{(\text{FNO})}$	$\mathcal{V}_{\text{err}}^{(\text{lin})} < \mathcal{V}_{\text{err}}^{(\text{DeepONet})}$
Free	2.233e-02 (1.23e-02)	1.226e-01 (6.608e-02)	2.258e-15 (1.739e-16)	1.956e-17	8.689e-18
Barrier	5.458e-02 (2.393e-02)	1.921e-01 (7.199e-02)	2.746e-15 (1.646e-16)	2.371e-21	3.134e-24
Harmonic Oscillator	5.315e-02 (1.902e-02)	1.429e-01 (6.499e-02)	2.856e-15 (1.056e-16)	4.301e-25	1.055e-20
Random	1.469e-02 (6.85e-03)	1.333e-01 (5.877e-02)	2.683e-15 (1.365e-16)	2.904e-20	2.949e-21
Paul Trap	9.285e-02 (4.017e-02)	6.62e-01 (5.152e-02)	3.158e-15 (4.277e-17)	1.363e-21	2.282e-56
Shaken Lattice	8.088e-02 (4.881e-03)	2.246e-01 (8.431e-02)	2.844e-15 (1.71e-16)	9.337e-62	3.392e-24
Gaussian Pulse	5.585e-02 (3.016e-02)	3.049e-01 (8.22e-02)	2.865e-15 (1.319e-16)	9.377e-18	1.347e-30
Coulomb	4.765e-02 (1.129e-02)	4.841e-02 (1.093e-02)	4.178e-15 (1.076e-15)	3.428e-33	3.619e-34
Dipole	4.361e-02 (7.814e-03)	5.228e-02 (1.280e-02)	2.281e-15 (2.539e-16)	6.865e-39	1.608e-32

K Compute Resources

All experiments involving the linear estimator were run on a standard-grade CPU. The deep learning-based approaches, namely the FNO and DeepONet, were trained on an Nvidia RTX 2080 Ti.